Am J Transl Res 2026;18(10):9336-9363
www.ajtr.org /ISSN:1943-8141/AJTR0175294

Original Article

OCT phenotype-guided structural and visual responses to intravitreal conbercept in diabetic macular edema: a retrospective cohort study

Yanlin Li, Xiangjun Li

Department of Ophthalmology, The Affiliated Hospital of Bei-hua University, Jilin 132011, Jilin, China

Received July 10, 2026; Accepted September 11, 2026; Epub October 15, 2026; Published October 30, 2026

Abstract: Purpose: To evaluate phenotype-specific trajectories of anatomical and visual responses, along with associated retinal and systemic biomarkers during intravitreal conbercept treatment for diabetic macular edema (DME). Methods: This single-center retrospective cohort study included 234 patients with 234 treatment-naïve eyes with center-involving DME, classified at baseline as pure diffuse retinal thickening (DRT; n = 60), pure cystoid macular edema (CME; n = 55), pure serous retinal detachment (SRD; n = 48), or mixed DME (n = 71). All eyes received three monthly conbercept injections followed by pro re nata (PRN) retreatment. Best-corrected visual acuity (BCVA), central macular thickness (CMT), subfoveal choroidal thickness (SFCT), ellipsoid zone (EZ) integrity, systemic immune-inflammation index (SII), and pan-immune-inflammation value (PIV) were assessed longitudinally, along with hyperreflective foci (HRF) and hard-exudate burden. Longitudinal analyses were performed using mixed-effects and generalized estimating equation models. Exploratory receiver operating characteristic and decision-curve analyses assessed baseline CMT, EZ integrity, and SII for 6-month visual improvement. Results: CMT decreased in all phenotypes, with a significant adjusted phenotype × time interaction ($P < 0.001$); proportional reductions were greatest in mixed DME and pure SRD. BCVA improved in all groups, with persistent phenotype-specific trajectories after adjustment ($P = 0.019$); pure DRT showed the greatest adjusted 6-month visual improvement. SFCT also decreased with a modest interaction ($P = 0.044$). Intact EZ prevalence increased from 44.0% to 74.4%, and 55.0% of eyes with baseline EZ disruption showed recovery at month 6. Manually assessed HRF counts decreased over follow-up, with exploratory correlations between HRF change and concurrent changes in CMT and BCVA. SII and PIV declined over time without phenotype-specific interactions; only SII remained weakly associated with repeated CMT. Baseline CMT, EZ integrity, and SII yielded AUCs of 0.61, 0.65, and 0.56, respectively, versus 0.69 for their combined model. Conclusions: Conbercept-treated DME showed substantial anatomical and visual improvement, but treatment trajectories differed by baseline OCT phenotype. Pure SRD and mixed DME showed greater anatomical responses, whereas pure DRT had the most favorable visual trajectory. Categorically assessed EZ integrity and manually counted HRF showed concurrent structural changes during follow-up, although their clinical utility remains to be determined; systemic inflammatory indices showed limited phenotype-specific or prognostic value.

Keywords: Diabetic macular edema, conbercept, optical coherence tomography, ellipsoid zone, hyperreflective foci

Introduction

Diabetic retinopathy (DR) continues to be a major cause of preventable visual impairment amid the rising global burden of diabetes. A systematic review and meta-analysis estimated that 103.1 million adults worldwide had DR in 2020, with the number projected to reach 160.5 million by 2045 [1]. Diabetic macular edema (DME), which can occur across the spectrum of DR, is a major cause of central visual loss. An OCT-based meta-analysis estimated that DME affects approximately 5.47% of people with diabetes, although prevalence varies across populations and diagnostic settings [2]. These estimates underscore the need not only for effective treatment but also for practical approaches to identifying heterogeneity in treatment response.

The pathogenesis of DME involves breakdown of the blood-retinal barrier, VEGF-mediated vascular permeability, extracellular fluid accumulation, neurovascular dysfunction, and inflam-

https://doi.org/10.62347/BZJB8903

matory activation. Intravitreal anti-VEGF therapy is recommended as first-line treatment for center-involving DME with visual impairment [3], with wide inter-eye variation in anatomical and functional responses [4]. Conbercept, a recombinant VEGF receptor fusion protein, has demonstrated sustained improvements in BCVA and retinal thickness in a phase III randomized trial and its 2-year extension [5]. However, average treatment effects do not fully capture the structural heterogeneity of DME or explain why marked retinal thinning may not translate into equivalent visual recovery.

OCT enables detailed characterization of this heterogeneity. Traditional morphologic patterns include DRT, CME, and SRD, but these components frequently coexist, resulting in mixed phenotypes that are often overlooked by hierarchical classification. Beyond CMT and fluid distribution, EZ integrity, HRF, DRIL, and other retinal features have been associated with visual outcomes after anti-VEGF therapy [6]. Nevertheless, current evidence is limited by heterogeneous biomarker definitions, cross-sectional assessments, inconsistent handling of mixed morphology, and incomplete adjustment for metabolic, ischemic, and treatment-related covariates. Longitudinal within-eye recovery of EZ integrity, changes in HRF and hard-exudate burden, and phenotype-specific changes in SFCT during anti-VEGF treatment also remain less well characterized.

Systemic inflammation may provide complementary information to local retinal imaging. Previous studies have linked CBC-derived inflammatory indices to OCT-defined DME severity and imaging features such as HRF and SRF [7]. PIV, which integrates neutrophil, monocyte, platelet, and lymphocyte counts, has also been associated with DME and selected OCT biomarkers [8]. It remains unclear whether SII and PIV exhibit phenotype-specific longitudinal changes, and if these changes are independently associated with structural or visual outcomes, or offer prognostic value beyond OCT markers.

Accordingly, this study evaluated 6-month anatomical and visual trajectories during intravitreal conbercept treatment across four mutually exclusive baseline OCT phenotypes: pure DRT, pure CME, pure SRD, and mixed DME. We additionally examined longitudinal changes in SFCT and EZ integrity, within-eye EZ recovery, HRF and hard-exudate burden, and systemic SII and PIV, together with systemic-ocular associations. Finally, we explored the discrimination and clinical utility of baseline CMT, EZ integrity, and SII, individually and in combination, for clinically meaningful visual improvement at month 6.

Methods

Study design and setting

This single-center retrospective cohort study enrolled consecutive patients with DME receiving intravitreal conbercept treatment at the Department of Ophthalmology, Affiliated Hospital of Beihua University, between January 2018 and February 2026. Potentially eligible patients were identified from the institutional electronic medical record and ophthalmic imaging systems. Clinical, laboratory, ophthalmic imaging, treatment, and follow-up data generated during routine clinical care were retrospectively extracted using a standardized data collection form. Patients were required to have baseline OCT images suitable for morphologic classification and sufficient follow-up records for assessment of the 6-month study outcomes.

The study evaluated longitudinal anatomical and visual responses according to baseline OCT phenotype and examined baseline clinical, retinal microstructural, and inflammatory factors associated with 6-month visual outcomes and anatomy-function mismatch. The study was conducted in accordance with the Declaration of Helsinki and reported in accordance with the Strengthening the Reporting of Observational Studies in Epidemiology (STROBE) statement [9]. The study protocol was approved by the Ethics Committee of the Affiliated Hospital of Beihua University (Approval No. 20260165). Because of the retrospective nature of the study and the use of routinely collected clinical data, the requirement for study-specific informed consent was waived by the Ethics Committee. All patients had provided written informed consent for intravitreal conbercept treatment before the procedure.

Study population

Consecutive patients were screened for eligibility during the study period. The index date

was defined as the date of the first intravitreal conbercept injection in the study eye. DME was diagnosed on the basis of a comprehensive ophthalmic evaluation, including dilated fundus examination, fundus fluorescein angiography (FFA), and spectral-domain optical coherence tomography (OCT).

Patients were eligible if they met all of the following criteria: (1) age ≥ 18 years; (2) a confirmed diagnosis of type 2 diabetes mellitus with center-involving DME in the study eye; (3) no previous intravitreal anti-vascular endothelial growth factor (anti-VEGF) or intravitreal corticosteroid treatment in the study eye; (4) initiation of conbercept treatment with three consecutive monthly loading injections followed by pro re nata (PRN) retreatment [10]; (5) availability of gradable baseline OCT images sufficient for OCT morphologic classification and quantitative assessment of retinal and choroidal structural biomarkers; (6) availability of baseline FFA of sufficient quality to evaluate macular ischemia; and (7) availability of clinical records sufficient to determine the 6-month visual and anatomical outcomes.

Patients were excluded if they met any of the following criteria: (1) participation in another interventional ophthalmic clinical trial within 3 months before the index injection or during the 6-month follow-up period; (2) cataract or other intraocular surgery within 6 months before the index injection, posterior capsulotomy within 2 months before the index injection, or intraocular surgery during the 6-month follow-up period; (3) substantial media opacity preventing reliable fundus examination, FFA grading, or OCT assessment; (4) history of retinal laser photocoagulation in the study eye; (5) concomitant ocular disorders that could independently cause macular edema or materially affect macular morphology, including retinal vein occlusion, age-related macular degeneration, or other retinal or choroidal vascular disorders; or (6) optic nerve disease or other ocular conditions that could materially affect visual acuity independently of DME.

Only one eye per patient was included. When only one eye fulfilled the eligibility criteria, that eye was selected. When both eyes fulfilled the criteria but conbercept treatment was initiated on different dates, the eye treated first was selected. When treatment was initiated in both eligible eyes on the same date, one eye was selected using a computer-generated random sequence. Accordingly, the unit of analysis was the individual patient eye, and adjustment for inter-eye correlation was not required.

OCT morphologic classification

Baseline OCT images were reviewed to identify three principal morphologic components of DME: diffuse retinal thickening (DRT), cystoid macular edema (CME), and serous retinal detachment (SRD), as previously described [11, 12].

DRT was defined as generalized thickening of the neurosensory retina with diffuse sponge-like areas of reduced intraretinal reflectivity. CME was defined by the presence of well-demarcated hyporeflective intraretinal cystoid spaces, predominantly involving the outer retinal layers. SRD was defined as separation of the neurosensory retina from the retinal pigment epithelium by an optically clear hyporeflective subretinal fluid space.

For the primary analysis, eyes were classified into four mutually exclusive OCT phenotype groups according to the combination of morphologic components present at baseline. Pure DRT was defined as DRT without CME or SRD; pure CME as CME without DRT or SRD; and pure SRD as SRD without DRT or CME. Eyes exhibiting two or more morphologic components were classified as mixed DME. Mixed DME was further characterized descriptively as DRT+CME, DRT+SRD, CME+SRD, or DRT+CME+SRD. Representative OCT images illustrating the principal morphologic features used for phenotype classification are shown in **Figure 1**.

Baseline OCT images were independently graded by two retinal specialists who were masked to follow-up visual outcomes, systemic inflammatory indices, and other clinical outcome data. Disagreements regarding the presence of individual morphologic components or the final OCT phenotype were adjudicated by a third senior retinal specialist. Intergrader agreement for the four-category OCT phenotype classification was assessed using Cohen's κ coefficient.

For sensitivity analyses, eyes were additionally reclassified using an alternative hierarchical

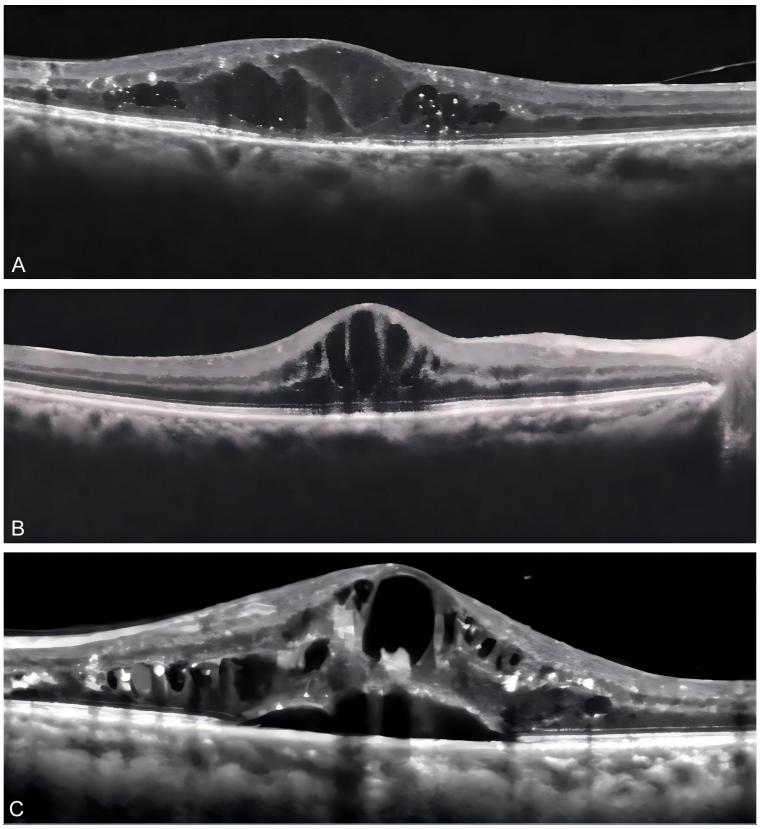


Figure 1. Representative optical coherence tomography morphologic features of diabetic macular edema. A. Diffuse retinal thickening pattern, showing generalized sponge-like thickening of the neurosensory retina with multiple small intraretinal hyporeflective spaces and no evident subretinal fluid. B. Cystoid macular edema pattern, characterized by prominent, well-demarcated intraretinal hyporeflective cystoid spaces with associated retinal thickening. C. Mixed diabetic macular edema exhibiting both cystoid macular edema and serous retinal detachment, with multiple intraretinal cystoid spaces and a hyporeflective subretinal fluid collection separating the neurosensory retina from the retinal pigment epithelium. These morphologic components were assessed individually and combined to define the pure DRT, pure CME, pure SRD, and mixed DME phenotypes used in the primary analysis. CME, cystoid macular edema; DME, diabetic macular edema; DRT, diffuse retinal thickening; OCT, optical coherence tomography; RPE, retinal pigment epithelium; SRD, serous retinal detachment.

three-group rule: eyes with DRT alone were classified as DRT; eyes with CME, including CME accompanied by DRT but without SRD, were classified as CME; and eyes with SRD, irrespective of accompanying DRT or CME, were classified as SRD.

Intravitreal conbercept treatment

All study eyes received intravitreal conbercept (0.5 mg/0.05 mL; Chengdu Kanghong Biotechnologies Co., Ltd., Chengdu, China; National Medical Products Administration approval No. S20130012). Treatment consisted of three consecutive monthly loading injections, with pro re nata (PRN) retreatments during the 6-month follow-up period [10]. After completion of the loading phase, retreatment decisions were made during routine follow-up according to clinical disease activity, primarily considering persistent or recurrent intraretinal or subretinal fluid and changes in central macular thickness on OCT together with changes in best-corrected visual acuity.

For each study eye, the date of every conbercept injection during follow-up was obtained from the treatment records. Injection exposure was summarized as the number of injections administered from baseline to month 1, from month 1 to month 3, and from month 3 to month 6, as well as the cumulative number of injections during the 6-month follow-up period.

Intravitreal injections were performed under aseptic conditions using topical anesthesia and ocular surface antisepsis with povidone-iodine in accordance with standard intravitreal injection procedures [13]. The eyelids and eyelashes were kept away from the injection site, and the injection was administered through the pars plana, approximately 3.5-4.0 mm posterior to the limbus according to lens status. After injection, patients were assessed for immediate procedure-related complications and subsequently followed according to the institutional intravitreal injection protocol.

Data collection, ophthalmic assessments, and imaging biomarkers

Demographic, systemic clinical, laboratory, and ophthalmic data were retrospectively extracted

from the medical records and imaging systems. Baseline variables included age, sex, duration of diabetes mellitus, duration of DME when ascertainable from the medical record, glycated hemoglobin (HbA1c), renal function, systemic glucose-lowering therapy, diabetic retinopathy (DR) severity, and baseline OCT phenotype. Diabetes duration was calculated from the first documented diagnosis of type 2 diabetes mellitus to the index date, and DME duration was calculated from the first documented diagnosis of DME in the study eye to the index date. For HbA1c and renal function, the measurement closest to and within 90 days before the index injection was used. Renal function was represented by the estimated glomerular filtration rate (eGFR) reported by the clinical laboratory. Baseline glucose-lowering therapy was recorded by pharmacologic class, including insulin, metformin, sulfonylureas, dipeptidyl peptidase-4 inhibitors, sodium-glucose cotransporter-2 inhibitors, glucagon-like peptide-1 receptor agonists, and other glucose-lowering agents, with multiple classes recorded when combination therapy was used. For multivariable analyses, glucose-lowering therapy was summarized as an insulin-containing regimen, non-insulin pharmacotherapy alone, or no pharmacologic treatment. DR severity was graded from baseline fundus findings as mild, moderate, or severe nonproliferative diabetic retinopathy or proliferative diabetic retinopathy according to the International Clinical Diabetic Retinopathy Disease Severity Scale [14]. Treatment dates and injection exposure were obtained as described in Section 2.4.

Ophthalmic assessments were obtained at baseline and at approximately 1, 3, and 6 months after the index injection. For consistency across retrospective data, the assessment closest to the target visit was selected within windows of ± 14 days for month 1, ± 21 days for month 3, and ± 30 days for month 6. Baseline ophthalmic measurements were obtained before the first conbercept injection. Best-corrected visual acuity (BCVA) was measured using a standard logarithmic visual acuity chart. Decimal visual acuity values were converted to logarithm of the minimum angle of resolution (logMAR) values for statistical analysis, with lower logMAR values indicating better visual acuity. Intraocular pressure was measured using a noncontact tonometer.

CMT, subfoveal choroidal thickness (SFCT), ellipsoid zone (EZ) integrity, external limiting membrane (ELM) integrity and disruption length, and disorganization of the retinal inner layers (DRIL) were evaluated using the Heidelberg confocal scanning laser ophthalmoscopy and OCT system (Heidelberg Engineering, Heidelberg, Germany). OCT examinations were performed using high-resolution macular scanning, with enhanced-depth imaging used for choroidal assessment. CMT was defined as retinal thickness at the center of the fovea. Automated retinal segmentation was reviewed and manually corrected when necessary. SFCT was measured vertically beneath the foveal center from the outer boundary of the retinal pigment epithelium-Bruch membrane complex to the choroid-sclera interface.

Baseline macular ischemia was evaluated from gradable fluorescein angiography obtained before initiation of conbercept treatment. Diabetic macular ischemia was graded according to the Early Treatment Diabetic Retinopathy Study-based classification as none, questionable, mild, moderate, or severe, considering the contour and enlargement of the foveal avascular zone and the extent of perifoveal capillary loss [15]. FFA images were independently graded by two retinal specialists who were masked to subsequent visual outcomes; disagreements were resolved by adjudication by a third senior retinal specialist.

EZ integrity was assessed at the individual-eye level at baseline and at months 1, 3, and 6. The EZ was classified as intact when a continuous hyperreflective EZ band was identifiable across the central foveal region and as disrupted when a definite focal or continuous interruption was present [16]. For each eye, longitudinal transitions were recorded as intact-to-intact, intact-to-disrupted, disrupted-to-intact, or disrupted-to-disrupted between baseline and each follow-up assessment. EZ recovery was defined as restoration of an intact EZ at a follow-up visit in an eye with EZ disruption at baseline.

ELM integrity was evaluated on the baseline OCT examination within the central 1-mm foveal region. The ELM was classified as intact when a continuous hyperreflective ELM line was identifiable across the evaluated region and as disrupted when one or more definite

interruptions were present. In eyes with ELM disruption, disruption length was quantified in micrometers as the cumulative horizontal extent of interrupted ELM segments within the central 1-mm foveal scan. Eyes with an intact ELM therefore had no measurable disruption length.

DRIL was defined as the inability to distinguish the boundaries between the ganglion cell-inner plexiform layer complex, inner nuclear layer, and outer plexiform layer within the central foveal region. Baseline DRIL extent was measured separately on the central horizontal and vertical OCT scans within the central 1-mm region. Horizontal and vertical DRIL extent were recorded in micrometers, and cumulative DRIL extent was calculated as the sum of the horizontal and vertical measurements.

ELM integrity, ELM disruption length, and horizontal and vertical DRIL extent were independently assessed by two retinal specialists who were masked to follow-up visual outcomes and systemic inflammatory indices. Disagreement regarding binary ELM integrity was resolved by adjudication by a third senior retinal specialist. Continuous ELM and DRIL measurements from the two graders were averaged for analysis.

Hyperreflective foci (HRF) were quantified on OCT at baseline and month 6. HRF were defined as discrete, well-circumscribed hyperreflective dots measuring approximately 20-40 μm [17]. HRF within the central 3-mm macular region, defined as 1.5 mm on either side of the foveal center, were manually counted and recorded separately for the inner retina, extending from the internal limiting membrane through the inner nuclear layer, and the outer retina, extending from the outer plexiform layer to the EZ [17]. The total HRF count was calculated as the sum of the inner- and outer-retinal counts. Larger hyperreflective lesions corresponding to clinically visible hard exudates on color fundus photography were not included in the HRF count.

Hard-exudate burden was assessed using gradable macula-centered color fundus photographs obtained at baseline and month 6. Hard exudates were identified as sharply demarcated yellow-white retinal deposits. Hard-exudate boundaries within a standardized ETDRS macular grid centered on the fovea were delineated on calibrated digital images, and the total hard-exudate area was quantified in mm^2 [18]. HRF counts and hard-exudate measurements were independently obtained by two retinal specialists who were masked to clinical outcomes and systemic inflammatory indices. Hard-exudate analyses were restricted to eyes with paired gradable baseline and month-6 photographs. Intergrader agreement was evaluated before the final measurements were entered into the analytical dataset.

Peripheral complete blood counts obtained during routine clinical care were retrieved at baseline and at the 1-, 3-, and 6-month follow-up assessments. When more than one complete blood count was available within a follow-up window, the sample obtained closest to the ophthalmic assessment was selected. The systemic immune-inflammation index (SII) was calculated as platelet count × neutrophil count/lymphocyte count, and the pan-immune-inflammation value (PIV) was calculated as neutrophil count × platelet count × monocyte count/lymphocyte count. All component cell counts used to calculate an index were required to originate from the same blood sample and assessment time point.

Outcomes

The co-primary outcomes were the longitudinal changes in best-corrected visual acuity (BCVA) and central macular thickness (CMT) from baseline through 6 months after initiation of intravitreal conbercept treatment. The principal comparisons assessed whether the trajectories of BCVA and CMT differed among the four baseline OCT phenotype groups: pure DRT, pure CME, pure SRD, and mixed DME.

Secondary outcomes included longitudinal changes in subfoveal choroidal thickness (SFCT), ellipsoid zone (EZ) integrity, systemic immune-inflammation index (SII), and pan-immune-inflammation value (PIV). EZ recovery was additionally evaluated among eyes with EZ disruption at baseline and was defined as restoration of an intact EZ at follow-up. Changes in local retinal imaging markers were evaluated from baseline to month 6 using total and layer-specific hyperreflective foci (HRF) counts and hard-exudate burden. Associations between changes in systemic inflammatory indices and

changes in ocular anatomical and imaging measures were also evaluated.

For the exploratory prognostic analysis, the primary prognostic outcome was visual response at month 6, defined as an improvement in BCVA of ≥ 0.20 logMAR from baseline. This magnitude of improvement corresponds approximately to a gain of ≥ 10 ETDRS letters, a threshold commonly used to characterize visual response in DME studies [19].

Anatomy-function mismatch was evaluated as a separate exploratory outcome at month 6. Anatomical response was defined as a > 20% reduction in CMT from baseline to month 6, whereas visual response was defined as an improvement in BCVA of ≥ 0.10 logMAR, approximately corresponding to a gain of ≥ 5 ETDRS letters. Anatomy-function mismatch was defined as an anatomical response accompanied by BCVA improvement of < 0.10 logMAR. Among eyes achieving an anatomical response, eyes meeting this definition were classified as having anatomy-function mismatch, whereas those with BCVA improvement of ≥ 0.10 logMAR were classified as concordant anatomical and visual responders.

For longitudinal change analyses, changes in CMT, SFCT, SII, PIV, HRF count, and hard-exudate burden were calculated as the follow-up value minus the baseline value. BCVA improvement was calculated as baseline logMAR BCVA minus follow-up logMAR BCVA so that a positive value represented visual improvement.

Statistical analysis

Statistical analyses were performed using IBM SPSS Statistics, version 27.0 (IBM Corp., Armonk, NY, USA) and R, version 4.5.1 (R Foundation for Statistical Computing, Vienna, Austria). All tests were two-sided, with $P < 0.05$ considered statistically significant. Continuous variables were summarized as mean ± SD or median (25th percentile, 75th percentile) according to distribution, and categorical variables as n (%). Baseline comparisons among the four OCT phenotypes used one-way analysis of variance, Welch's analysis of variance, or the Kruskal-Wallis H test for continuous variables and the Pearson χ^2 or Fisher's exact test for categorical variables, as appropriate. Significant overall four-group comparisons were followed by Bonferroni-adjusted pairwise tests.

Intergrader agreement was assessed before final imaging measurements were entered into the analytical dataset. Cohen's κ was used for OCT phenotype and ELM integrity, weighted κ for macular ischemia grade, and two-way random-effects, absolute-agreement intraclass correlation coefficients for ELM disruption length, horizontal and vertical DRIL extent, HRF counts, and hard-exudate area. Continuous imaging measurements were averaged across the two graders for analysis. Cumulative DRIL extent was calculated as the sum of horizontal and vertical DRIL extent.

Longitudinal BCVA, CMT, SFCT, SII, and PIV were analyzed using mixed-effects models with a patient-specific random intercept and fixed effects for OCT phenotype, categorical assessment time, and phenotype × time interaction. CMT, SFCT, SII, and PIV were natural log-transformed because of right-skewness; BCVA was analyzed on the logMAR scale. Model-based contrasts evaluated within-phenotype changes and between-phenotype differences at individual visits, with Bonferroni adjustment where applicable. Model assumptions were assessed using residual distributions and diagnostic plots.

Adjustment of the principal longitudinal trajectories was performed sequentially. Model 1 included phenotype, time, and phenotype × time. Model 2 additionally included age, sex, diabetes duration, HbA1c, and baseline systemic glucose-lowering therapy. Model 3 further included eGFR, diabetic retinopathy severity, and macular ischemia. Model 4 additionally incorporated baseline EZ integrity, ELM disruption length, cumulative DRIL extent and total HRF count, and served as the principal structural-adjusted model. Model 5 further included cumulative conbercept injection number before each follow-up assessment as a time-varying treatment-exposure covariate. Diabetic retinopathy severity was modeled ordinally, and macular ischemia was dichotomized as, none/questionable/mild versus moderate/severe.

EZ integrity was analyzed as a repeated binary outcome using generalized estimating equations with a binomial distribution, logit link,

patient-level clustering, and exchangeable working correlation. Individual-eye transitions from baseline to months 1, 3, and 6 were tabulated, and among eyes with baseline EZ disruption, visit-specific recovery was analyzed using a separate binomial GEE model. HRF counts from baseline to month 6 were analyzed using negative-binomial GEE, whereas hard-exudate burden was analyzed using a linear mixed-effects model after log (1 + x) transformation when required.

Systemic-ocular associations were examined using Spearman correlations between 6-month changes in SII or PIV and changes in CMT, HRF, and hard-exudate burden. Separate longitudinal mixed-effects models then related time-varying log-transformed SII or PIV to repeated log-transformed CMT or BCVA, adjusting for phenotype, time, age, sex, diabetes duration, HbA1c, eGFR, macular ischemia, and glucose-lowering therapy.

Two classification sensitivity analyses were performed. First, principal longitudinal analyses were repeated after excluding mixed DME. Second, eyes were reclassified using an alternative hierarchical scheme in which DRT+CME without SRD was assigned to CME and all SRD-containing eyes were assigned to SRD. These analyses used the covariate structure of Model 4.

Exploratory prognostic analyses evaluated clinically meaningful visual improvement at month 6, defined as BCVA improvement ≥ 0.20 logMAR. Baseline CMT, EZ integrity, ELM disruption length, cumulative DRIL extent, and SII were evaluated individually using univariable logistic regression and fixed-time ROC analysis. ELM disruption length was coded as 0 μm when the ELM was intact. In addition to the CMT+EZ+SII model, an extended structural model included CMT, EZ integrity, ELM disruption length, and cumulative DRIL extent, and an integrated model additionally included natural log-transformed SII. Discrimination was summarized using AUCs with 95% CIs. DCA was retained for the prespecified CMT, EZ, SII, and CMT+EZ+SII models.

Anatomy-function mismatch was evaluated separately. Anatomical response was defined as > 20% CMT reduction from baseline to month 6, and visual response as BCVA improvement ≥ 0.10 logMAR, approximately equivalent to ≥ 5 ETDRS letters. Mismatch was defined as anatomical response accompanied by < 0.10-logMAR BCVA improvement. Among anatomical responders, baseline ELM, DRIL, EZ, HRF, BCVA, CMT, macular ischemia, and phenotype were compared between mismatch and concordant responders. A parsimonious multivariable logistic regression model evaluated mismatch using ELM disruption length and cumulative DRIL extent as the principal structural predictors, with adjustment for baseline BCVA, baseline CMT, macular ischemia, and OCT phenotype. ELM and DRIL effects were expressed per 100-μm increase.

Missingness was examined for each variable and visit. Longitudinal mixed-effects and GEE models used all available observations under their respective assumptions. Predictor variables with ≤ 20% missingness were handled using multiple imputation by chained equations with 30 datasets; variables with > 20% missingness were excluded from multivariable models. Month-6 prognostic and mismatch analyses required observed month-6 outcomes. Complete-case analyses were performed as sensitivity analyses for the principal adjusted models.

Results

Patient selection, baseline characteristics, and OCT phenotype distribution

Of 437 patients screened, 203 were excluded and 234 patients with 234 study eyes were included (**Figure 2**). Baseline OCT phenotypes comprised 60 pure DRT eyes (25.6%), 55 pure CME (23.5%), 48 pure SRD (20.5%), and 71 mixed DME (30.3%); mixed-pattern composition is shown in Supplementary Table 1. Intergrader agreement was high for all imaging parameters: OCT phenotype classification (κ = 0.86, 95% CI 0.81-0.91), macular ischemia grading (weighted κ = 0.82, 95% CI 0.77-0.87), ELM integrity (κ = 0.89, 95% CI 0.84-0.94), ELM disruption length (ICC = 0.94, 95% CI 0.92-0.96), horizontal and vertical DRIL extent (ICC = 0.92, 95% CI 0.90-0.94 and ICC = 0.91, 95% CI 0.89-0.93, respectively), HRF count (ICC = 0.93, 95% CI 0.91-0.95), and hard-exudate area (ICC = 0.90, 95% CI 0.87-0.92).

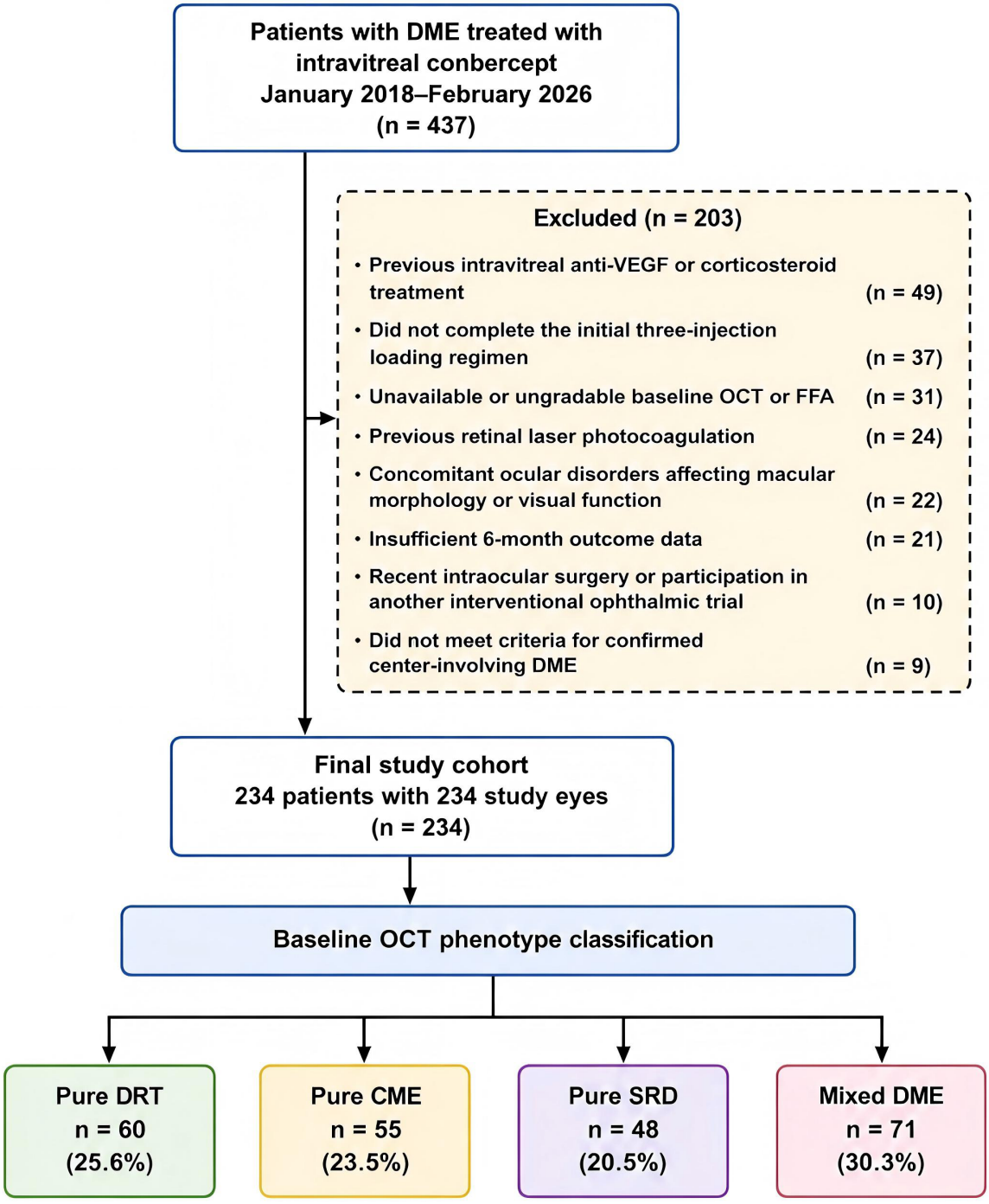


Figure 2. Patient selection and OCT phenotype classification flowchart. Among 437 patients with diabetic macular edema who received intravitreal conbercept between January 2018 and February 2026, 203 were excluded: 49 had received previous intravitreal anti-VEGF or corticosteroid treatment, 37 did not complete the initial three-injection loading regimen, 31 had unavailable or ungradable baseline OCT or FFA, 24 had undergone previous retinal laser photocoagulation, 22 had concomitant ocular disorders that could affect macular morphology or visual function, 21 lacked sufficient 6-month outcome data, 10 had recent intraocular surgery or participation in another interventional ophthalmic trial, and 9 did not meet the criteria for confirmed center-involving DME. The final cohort comprised 234 patients with 234 study eyes: 60 pure DRT, 55 pure CME, 48 pure SRD, and 71 mixed DME. Anti-VEGF, anti-vascular endothelial growth factor; CME, cystoid macular edema; DME, diabetic macular edema; DRT, diffuse retinal thickening; FFA, fundus fluorescein angiography; OCT, optical coherence tomography; SRD, serous retinal detachment.

Table 1. Baseline characteristics according to OCT phenotype

Characteristic	Overall (N = 234)	Pure DRT (n = 60)	Pure CME (n = 55)	Pure SRD (n = 48)	Mixed DME (n = 71)	Test statistic	*p* value
Age, years	59.8 ± 8.6	61.7 ± 8.6	59.3 ± 8.4	58.7 ± 9.0	59.3 ± 8.3	F = 1.324	0.267
Male sex, n (%)	124 (53.0)	31 (51.7)	29 (52.7)	24 (50.0)	40 (56.3)	χ^2 = 0.535	0.911
Diabetes duration, years	10.1 (7.4, 12.7)	10.0 (6.9, 12.7)	10.7 (8.4, 12.4)	8.8 (6.7, 11.7)	9.6 (7.8, 13.7)	H = 2.764	0.430
HbA1c, %	8.2 ± 1.1	8.2 ± 1.1	8.2 ± 1.0	8.0 ± 1.1	8.3 ± 1.1	F = 0.455	0.714
DME duration, months	8.4 (5.3, 14.0)	9.8 (5.5, 14.5)	8.3 (5.7, 14.3)	7.2 (5.2, 12.3)	8.2 (4.4, 14.4)	H = 2.965	0.397
eGFR, mL/min/1.73 m^2	77.2 ± 15.3	75.6 ± 12.8	77.1 ± 15.6	79.3 ± 16.7	77.3 ± 16.2	F = 0.488	0.691
Systemic glucose-lowering therapy, n (%)						χ^2 = 4.521	0.607
Insulin-containing regimen	103 (44.0)	20 (33.3)	26 (47.3)	24 (50.0)	33 (46.5)		
Non-insulin pharmacotherapy alone	106 (45.3)	33 (55.0)	24 (43.6)	18 (37.5)	31 (43.7)		
No pharmacologic treatment	25 (10.7)	7 (11.7)	5 (9.1)	6 (12.5)	7 (9.9)		
DR severity, n (%)						χ^2 = 8.328	0.501
Mild NPDR	32 (13.7)	12 (20.0)	9 (16.4)	4 (8.3)	7 (9.9)		
Moderate NPDR	86 (36.8)	23 (38.3)	20 (36.4)	15 (31.2)	28 (39.4)		
Severe NPDR	78 (33.3)	19 (31.7)	18 (32.7)	17 (35.4)	24 (33.8)		
PDR	38 (16.2)	6 (10.0)	8 (14.5)	12 (25.0)	12 (16.9)		
Macular ischemia grade, n (%)						χ^2 = 12.818	0.382
None	74 (31.6)	21 (35.0)	18 (32.7)	19 (39.6)	16 (22.5)		
Questionable	27 (11.5)	9 (15.0)	6 (10.9)	6 (12.5)	6 (8.5)		
Mild	68 (29.1)	16 (26.7)	15 (27.3)	13 (27.1)	24 (33.8)		
Moderate	49 (20.9)	11 (18.3)	15 (27.3)	6 (12.5)	17 (23.9)		
Severe	16 (6.8)	3 (5.0)	1 (1.8)	4 (8.3)	8 (11.3)		
BCVA, logMAR	0.77 (0.59, 0.93)	0.69 (0.58, 0.84)	0.79 (0.59, 0.92)	0.78 (0.64, 0.96)	0.80 (0.59, 0.97)	H = 6.519	0.089
CMT, μm	455.3 (360.0, 535.1)	356.8 (299.2, 400.9)	432.5 (354.5, 477.3)	496.6 (388.6, 544.1)	562.4 (473.9, 605.7)	H = 96.874	< 0.001
SFCT, μm	324.4 (296.9, 355.5)	311.0 (289.7, 334.0)	323.4 (296.4, 355.9)	328.0 (305.7, 362.6)	333.4 (304.2, 368.8)	H = 8.229	0.042
EZ integrity, n (%)						χ^2 = 23.086	< 0.001
Intact	103 (44.0)	40 (66.7)	27 (49.1)	17 (35.4)	19 (26.8)		
Disrupted	131 (56.0)	20 (33.3)	28 (50.9)	31 (64.6)	52 (73.2)		
ELM integrity, n (%)						χ^2 = 9.649	0.022
Intact	128 (54.7)	42 (70.0)	31 (56.4)	24 (50.0)	31 (43.7)		
Disrupted	106 (45.3)	18 (30.0)	24 (43.6)	24 (50.0)	40 (56.3)		
ELM disruption length, μm‡	369.4 (276.5, 483.3)	317.3 (189.5, 370.5)	360.2 (259.8, 496.6)	350.9 (306.9, 468.9)	413.0 (338.4, 530.5)	H = 10.767	0.013
Horizontal DRIL extent, μm	218.1 (137.1, 316.1)	153.6 (121.1, 251.8)	216.4 (156.5, 286.5)	254.1 (145.2, 333.1)	250.0 (165.9, 373.6)	H = 14.173	0.003
Vertical DRIL extent, μm	194.1 (137.8, 274.4)	164.5 (118.9, 214.7)	194.5 (149.0, 266.4)	202.2 (158.0, 324.8)	206.8 (150.5, 352.1)	H = 11.997	0.007
Cumulative DRIL extent, μm§	415.4 (286.4, 588.2)	324.0 (240.8, 460.7)	410.8 (307.5, 554.3)	442.2 (308.5, 650.6)	467.4 (328.5, 716.2)	H = 13.812	0.003
Total HRF count	23.0 (16.0, 30.0)	16.0 (11.0, 21.0)	20.0 (15.0, 26.5)	26.5 (21.5, 33.2)	28.0 (21.0, 38.0)	H = 58.161	< 0.001
Hard-exudate area, $mm^{2†}$	0.54 (0.27, 1.11)	0.57 (0.24, 1.07)	0.34 (0.26, 0.78)	0.47 (0.21, 1.31)	0.73 (0.39, 1.17)	H = 6.301	0.098
SII	596.93 (467.48, 814.17)	594.36 (482.80, 726.48)	656.18 (495.95, 833.36)	586.54 (463.09, 744.60)	603.28 (424.96, 839.54)	H = 2.733	0.435
PIV	236.38 (169.51, 319.69)	222.91 (177.75, 304.31)	225.88 (158.96, 318.24)	259.35 (176.46, 318.80)	239.03 (173.30, 324.18)	H = 1.562	0.668

Notes: Data are presented as mean ± SD, median (25th percentile, 75th percentile), or n (%), as appropriate. One-way analysis of variance was used for approximately normally distributed continuous variables and the Kruskal-Wallis H test for non-normally distributed variables. Categorical variables were compared using the Pearson χ^2 test or Fisher's exact test, as appropriate. Bonferroni adjustment was applied to post hoc pairwise comparisons following a significant overall test. For CMT, all six pairwise comparisons remained statistically significant after adjustment. For SFCT, only the comparison between pure DRT and mixed DME remained significant (adjusted P = 0.031). For baseline EZ integrity, significant adjusted pairwise differences were observed between pure DRT and pure SRD and between pure DRT and mixed DME. For ELM integrity, the difference between pure DRT and mixed DME remained significant (adjusted P = 0.026). For ELM disruption length, the pure DRT versus mixed DME comparison remained significant (adjusted P = 0.010). For horizontal DRIL extent, pure DRT differed significantly from mixed DME (adjusted P = 0.003). For vertical DRIL extent, pure DRT differed from pure SRD (adjusted P = 0.047) and mixed DME (adjusted P = 0.013). For cumulative DRIL extent, pure DRT differed from pure SRD (adjusted P = 0.035) and mixed DME (adjusted P = 0.004). Diabetes duration was available for 229 patients, HbA1c for 226, DME duration for 218, and eGFR for 229. †Hard-exudate measurements were available for 216 eyes with paired gradable baseline and month-6 color fundus photographs (pure DRT, n = 56; pure CME, n = 51; pure SRD, n = 44; mixed DME, n = 65). ‡ELM disruption length was summarized among the 106 eyes with baseline ELM disruption (pure DRT, n = 18; pure CME, n = 24; pure SRD, n = 24; mixed DME, n = 40). §Cumulative DRIL extent was calculated as the sum of horizontal and vertical DRIL extent. All other variables shown were available for the full baseline cohort. BCVA, best-corrected visual acuity; CME, cystoid macular edema; CMT, central macular thickness; DME, diabetic macular edema; DR, diabetic retinopathy; DRIL, disorganization of the retinal inner layers; DRT, diffuse retinal thickening; eGFR, estimated glomerular filtration rate; ELM, external limiting membrane; EZ, ellipsoid zone; HbA1c, glycated hemoglobin; HRF, hyperreflective foci; logMAR, logarithm of the minimum angle of resolution; NPDR, nonproliferative diabetic retinopathy; OCT, optical coherence tomography; PDR, proliferative diabetic retinopathy; PIV, pan-immune-inflammation value; SFCT, subfoveal choroidal thickness; SII, systemic immune-inflammation index; SRD, serous retinal detachment.

Table 2. Conbercept treatment exposure during the 6-month follow-up according to baseline OCT phenotype

Treatment exposure	Overall (N = 234)	Pure DRT (n = 60)	Pure CME (n = 55)	Pure SRD (n = 48)	Mixed DME (n = 71)	Test statistic	*p* value
Interval injection number							
Baseline to M1	2 (2, 2)	2 (2, 2)	2 (2, 2)	2 (2, 2)	2 (2, 2)	-	-
M1 to M3	1 (1, 2)	1 (1, 2)	1 (1, 2)	1 (1, 2)	1 (1, 2)	H = 1.814	0.612
M3 to M6	1 (1, 2)	1 (1, 2)	1 (1, 2)	1 (1, 2)	1 (1, 2)	H = 2.817	0.421
Cumulative injection number							
Through M1	2 (2, 2)	2 (2, 2)	2 (2, 2)	2 (2, 2)	2 (2, 2)	-	-
Through M3	3 (3, 4)	3 (3, 4)	3 (3, 4)	3 (3, 4)	3 (3, 4)	H = 1.814	0.612
Through M6	5 (4, 5)	5 (4, 5)	5 (4, 5)	5 (4, 5)	5 (4, 5)	H = 3.920	0.270
Through M6, mean ± SD	4.68 ± 0.80	4.53 ± 0.79	4.62 ± 0.80	4.77 ± 0.81	4.79 ± 0.81	-	-
Total injections through M6, n (%)						χ^2 = 4.594	0.868
3 injections	14 (6.0)	5 (8.3)	4 (7.3)	2 (4.2)	3 (4.2)		
4 injections	83 (35.5)	24 (40.0)	20 (36.4)	16 (33.3)	23 (32.4)		
5 injections	101 (43.2)	25 (41.7)	24 (43.6)	21 (43.8)	31 (43.7)		
6 injections	36 (15.4)	6 (10.0)	7 (12.7)	9 (18.8)	14 (19.7)		

Notes: Injection counts are presented as median (25th percentile, 75th percentile), mean ± SD, or n (%), as indicated. The index injection was included in the baseline-to-month-1 and cumulative injection counts. All included eyes completed the three consecutive monthly loading injections. Subsequent injections were administered according to PRN retreatment criteria. Between-group comparisons of injection counts were performed using the Kruskal-Wallis H test; the distribution of total 6-month injection numbers was compared using the Pearson χ^2 test. CME, cystoid macular edema; DME, diabetic macular edema; DRT, diffuse retinal thickening; M1, month 1; M3, month 3; M6, month 6; OCT, optical coherence tomography; PRN, pro re nata; SRD, serous retinal detachment.

Demographic and systemic characteristics, including age, sex, diabetes and DME duration, HbA1c, eGFR, glucose-lowering therapy, DR severity, and macular ischemia, were comparable across phenotypes (all P > 0.05) (**Table 1**). Baseline BCVA was also similar (P = 0.089). In contrast, CMT differed markedly among phenotypes (H = 96.874, P < 0.001), increasing from pure DRT to pure CME, pure SRD, and mixed DME; all pairwise comparisons were significant after Bonferroni adjustment. SFCT showed a smaller overall difference (H = 8.229, P = 0.042). Baseline EZ integrity (χ^2 = 23.086, P < 0.001) and HRF count (H = 58.161, P < 0.001) also differed among phenotypes.

ELM integrity differed among phenotypes (χ^2 = 9.649, P = 0.022), with an intact ELM present in 128 eyes (54.7%) overall. Among eyes with ELM disruption, disruption length also differed among phenotypes (H = 10.767, P = 0.013). Horizontal, vertical, and cumulative DRIL extent showed significant overall between-phenotype differences (H = 14.173, P = 0.003; H = 11.997, P = 0.007; and H = 13.812, P = 0.003, respectively). Hard-exudate burden, SII, and PIV did not differ among phenotypes (all P > 0.05).

Conbercept treatment exposure during follow-up

All 234 eyes completed the three-injection loading regimen. The median cumulative injection number was 3 (3, 4) by month 3, and 5 (4, 5) by month 6 (**Table 2**). Six-month mean cumulative exposure ranged from 4.53 ± 0.79 injections in pure DRT to 4.79 ± 0.81 in mixed DME, without a significant between-phenotype difference (H = 3.920, P = 0.270). Overall, 14 (6.0%), 83 (35.5%), 101 (43.2%), and 36 eyes (15.4%) received 3, 4, 5, and 6 injections, respectively; this distribution was also comparable among phenotypes (χ^2 = 4.594, P = 0.868).

Changes in central macular thickness

CMT decreased significantly over 6 months in all four OCT phenotypes (**Table 3**). The unadjusted mixed-effects model showed a significant phenotype × time interaction (Wald χ^2 = 156.42, P < 0.001), with significant reductions from baseline at months 1, 3, and 6 in every group (all Bonferroni-adjusted P < 0.001).

The difference between baseline and month-6 group medians was greatest in mixed DME

Table 3. Changes in central macular thickness during follow-up according to baseline OCT phenotype

Time point/change	Pure DRT (n = 60), μm	Pure CME (n = 55), μm	Pure SRD (n = 48), μm	Mixed DME (n = 71), μm	H statistic	Overall *p* value
Observed CMT						
Baseline	356.8 (299.2, 400.9)	432.5 (354.5, 477.3)	496.6 (388.6, 544.1)	562.4 (473.9, 605.7)	96.874	< 0.001
Month 1	307.5 (271.2, 350.8)	353.0 (301.5, 397.0)	401.0 (329.0, 466.5)	435.0 (356.0, 514.0)	63.428	< 0.001
Month 3	282.0 (249.0, 317.0)	311.0 (269.0, 344.0)	338.5 (283.0, 390.0)	368.0 (303.0, 425.0)	34.615	< 0.001
Month 6	270.5 (241.0, 300.0)	289.0 (254.0, 321.0)	305.0 (263.0, 346.0)	323.0 (274.0, 373.0)	18.760	< 0.001
Difference between observed group medians (follow-up - baseline)						
Baseline → Month 1	-49.3	-79.5	-95.6	-127.4	-	-
Baseline → Month 3	-74.8	-121.5	-158.1	-194.4	-	-
Baseline → Month 6	-86.3	-143.5	-191.6	-239.4	-	-
Adjusted geometric mean ratio vs baseline (95% CI)						
Month 1/baseline	0.86 (0.83-0.89)	0.82 (0.79-0.85)	0.80 (0.77-0.83)	0.78 (0.75-0.81)	-	< 0.001†
Month 3/baseline	0.79 (0.76-0.82)	0.72 (0.69-0.75)	0.68 (0.65-0.71)	0.66 (0.63-0.69)	-	< 0.001†
Month 6/baseline	0.76 (0.73-0.79)	0.67 (0.64-0.70)	0.61 (0.58-0.64)	0.58 (0.56-0.61)	-	< 0.001†

Notes: Observed CMT values are presented as median (25th percentile, 75th percentile). Absolute changes were calculated as the follow-up median minus the baseline median and are provided descriptively. Between-phenotype comparisons at individual time points were performed using the Kruskal-Wallis H test. Longitudinal CMT trajectories were evaluated using linear mixed-effects models fitted to natural log-transformed CMT values, with a patient-specific random intercept. The unadjusted phenotype × time interaction was significant (Wald $\chi^2 = 156.42$, $P < 0.001$). Adjusted geometric mean ratios were obtained from the principal multivariable model controlling for age, sex, diabetes duration, HbA1c, systemic glucose-lowering therapy, eGFR, diabetic retinopathy severity, macular ischemia, baseline EZ integrity, and baseline HRF count; the adjusted phenotype × time interaction remained significant (Wald $\chi^2 = 128.63$, $P < 0.001$). †*p* values refer to the within-phenotype contrast with baseline; all remained significant after Bonferroni adjustment. CI, confidence interval; CME, cystoid macular edema; CMT, central macular thickness; DME, diabetic macular edema; DRT, diffuse retinal thickening; eGFR, estimated glomerular filtration rate; EZ, ellipsoid zone; HbA1c, glycated hemoglobin; HRF, hyperreflective foci; OCT, optical coherence tomography; SRD, serous retinal detachment.

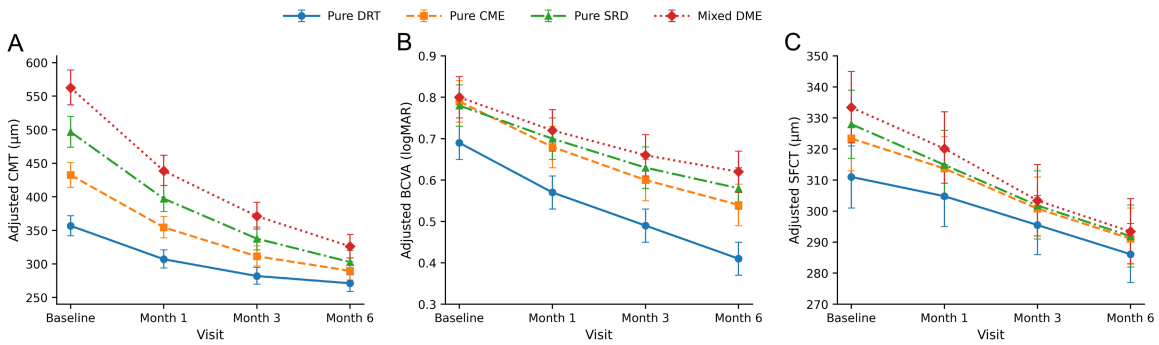


Figure 3. Adjusted longitudinal trajectories of central macular thickness, best-corrected visual acuity, and subfoveal choroidal thickness according to baseline OCT phenotype during 6 months of intravitreal conbercept treatment. A. Adjusted central macular thickness (CMT) trajectories. Values are back-transformed geometric means with 95% confidence intervals derived from the linear mixed-effects model fitted to natural log-transformed CMT. The OCT phenotype × time interaction was statistically significant (Wald $\chi^2 = 128.63$, $P < 0.001$). B. Adjusted best-corrected visual acuity (BCVA) trajectories. Values are estimated marginal means with 95% confidence intervals on the logMAR scale; lower logMAR values indicate better visual acuity. The OCT phenotype × time interaction was statistically significant (Wald $\chi^2 = 19.78$, $P = 0.019$). C. Adjusted subfoveal choroidal thickness (SFCT) trajectories. Values are back-transformed geometric means with 95% confidence intervals derived from the linear mixed-effects model fitted to natural log-transformed SFCT. The OCT phenotype × time interaction was statistically significant (Wald $\chi^2 = 17.30$, $P = 0.044$). All models were adjusted for age, sex, diabetes duration, HbA1c, systemic glucose-lowering therapy, estimated glomerular filtration rate, diabetic retinopathy severity, macular ischemia, baseline ellipsoid zone integrity, and baseline hyperreflective foci count. BCVA, best-corrected visual acuity; CI, confidence interval; CME, cystoid macular edema; CMT, central macular thickness; DME, diabetic macular edema; DRT, diffuse retinal thickening; eGFR, estimated glomerular filtration rate; EZ, ellipsoid zone; HbA1c, glycated hemoglobin; HRF, hyperreflective foci; logMAR, logarithm of the minimum angle of resolution; OCT, optical coherence tomography; SFCT, subfoveal choroidal thickness; SRD, serous retinal detachment.

(-239.4 μm), followed by pure SRD (-191.6 μm), pure CME (-143.5 μm), and pure DRT (-86.3 μm). Between-phenotype differences persisted at month 6 ($H = 18.76$, $P < 0.001$); mixed DME remained thicker than pure DRT (adjusted $P < 0.001$) and pure CME (adjusted $P = 0.018$), whereas other pairwise comparisons were not significant.

After additional adjustment for baseline EZ integrity, ELM disruption length, cumulative DRIL extent, and HRF count, the phenotype × time interaction remained significant (Wald $\chi^2 = 120.72$, $P < 0.001$). Adjusted trajectories from the principal structural-adjusted model are shown in **Figure 3A**.

Changes in best-corrected visual acuity

BCVA improved significantly over the 6-month follow-up in all four OCT phenotype groups (**Table 4**). The unadjusted mixed-effects model showed significant effects of time (Wald $\chi^2 = 214.63$, $P < 0.001$) and phenotype × time (Wald $\chi^2 = 29.84$, $P < 0.001$). Within each phenotype, BCVA improved significantly from baseline at months 1, 3, and 6 (all Bonferroni-adjusted $P < 0.001$).

BCVA was comparable among phenotypes at baseline and month 1 (both $P > 0.05$). At month 3, pure DRT showed better BCVA than mixed DME (adjusted $P = 0.019$). By month 6, the overall difference was significant ($H = 25.460$, $P < 0.001$); pure DRT had better BCVA than pure SRD (adjusted $P = 0.004$) and mixed DME (adjusted $P < 0.001$), and pure CME had better BCVA than mixed DME (adjusted $P = 0.038$).

After multivariable adjustment including baseline retinal microstructural characteristics, the phenotype × time interaction remained significant but was attenuated (Wald $\chi^2 = 17.70$, $P = 0.039$). Adjusted month-6 improvements were 0.26, 0.24, 0.20, and 0.18 logMAR in pure DRT, pure CME, pure SRD, and mixed DME, respectively (**Figure 3B**).

Changes in subfoveal choroidal thickness

SFCT decreased over 6 months in all four OCT phenotype groups (**Table 5**). The unadjusted mixed-effects model showed a significant time effect (Wald $\chi^2 = 186.72$, $P < 0.001$) and phenotype × time interaction (Wald $\chi^2 = 19.40$, $P = 0.022$). SFCT was significantly lower than base-

Table 4. Changes in best-corrected visual acuity during follow-up according to baseline OCT phenotype

Time point/change	Pure DRT (n = 60), logMAR	Pure CME (n = 55), logMAR	Pure SRD (n = 48), logMAR	Mixed DME (n = 71), logMAR	H statistic	Overall *p* value
Observed BCVA						
Baseline	0.69 (0.58, 0.84)	0.79 (0.59, 0.92)	0.78 (0.64, 0.96)	0.80 (0.59, 0.97)	6.519	0.089
Month 1	0.56 (0.44, 0.70)	0.65 (0.50, 0.80)	0.67 (0.52, 0.82)	0.69 (0.53, 0.85)	6.104	0.107
Month 3	0.48 (0.36, 0.61)	0.56 (0.42, 0.70)	0.59 (0.45, 0.73)	0.62 (0.47, 0.77)	10.720	0.013
Month 6	0.41 (0.30, 0.54)	0.49 (0.36, 0.63)	0.55 (0.42, 0.69)	0.58 (0.44, 0.73)	25.460	< 0.001
Difference between observed group medians (baseline - follow-up)†						
Baseline → Month 1	0.13	0.14	0.11	0.11	-	-
Baseline → Month 3	0.21	0.23	0.19	0.18	-	-
Baseline → Month 6	0.28	0.30	0.23	0.22	-	-
Adjusted mean change from baseline‡ (95% CI)						
Month 1 - baseline	-0.12 (-0.15 to -0.09)	-0.11 (-0.14 to -0.08)	-0.09 (-0.12 to -0.06)	-0.08 (-0.11 to -0.05)	-	< 0.001§
Month 3 - baseline	-0.21 (-0.24 to -0.18)	-0.19 (-0.22 to -0.16)	-0.16 (-0.20 to -0.12)	-0.14 (-0.17 to -0.11)	-	< 0.001§
Month 6 - baseline	-0.28 (-0.32 to -0.24)	-0.25 (-0.29 to -0.21)	-0.20 (-0.24 to -0.16)	-0.18 (-0.21 to -0.15)	-	< 0.001§

Notes: Observed BCVA values are presented as median (25th percentile, 75th percentile). Lower logMAR values indicate better visual acuity. †Observed median improvement was calculated as the baseline median minus the corresponding follow-up median and is presented descriptively. Between-phenotype comparisons at individual time points were performed using the Kruskal-Wallis H test. Following a significant overall comparison, pairwise comparisons were performed with Bonferroni adjustment. At month 3, only pure DRT versus mixed DME remained significant (adjusted P = 0.019). At month 6, significant comparisons were pure DRT versus pure SRD (adjusted P = 0.004), pure DRT versus mixed DME (adjusted P < 0.001), and pure CME versus mixed DME (adjusted P = 0.038); the remaining pairwise comparisons were not significant. ‡Adjusted changes were estimated from the principal linear mixed-effects model controlling for age, sex, diabetes duration, HbA1c, systemic glucose-lowering therapy, eGFR, diabetic retinopathy severity, macular ischemia, baseline EZ integrity, and baseline HRF count. The adjusted OCT phenotype × time interaction was significant (Wald χ^2 = 19.78, P = 0.019). §*p* values represent the within-phenotype contrast with baseline; all remained significant after Bonferroni adjustment. BCVA, best-corrected visual acuity; CI, confidence interval; CME, cystoid macular edema; DME, diabetic macular edema; DRT, diffuse retinal thickening; eGFR, estimated glomerular filtration rate; EZ, ellipsoid zone; HbA1c, glycated hemoglobin; HRF, hyperreflective foci; logMAR, logarithm of the minimum angle of resolution; OCT, optical coherence tomography; SRD, serous retinal detachment.

Table 5. Changes in subfoveal choroidal thickness during follow-up according to baseline OCT phenotype

Time point/change	Pure DRT (n = 60), μm	Pure CME (n = 55), μm	Pure SRD (n = 48), μm	Mixed DME (n = 71), μm	H statistic	Overall *p* value
Observed SFCT						
Baseline	311.0 (289.7, 334.0)	323.4 (296.4, 355.9)	328.0 (305.7, 362.6)	333.4 (304.2, 368.8)	8.229	0.042
Month 1	304.0 (282.0, 328.0)	313.0 (289.0, 343.0)	316.0 (295.0, 348.0)	320.0 (294.0, 355.0)	7.486	0.058
Month 3	295.0 (273.0, 318.0)	300.0 (278.0, 330.0)	302.0 (281.0, 333.0)	304.0 (279.0, 338.0)	5.836	0.120
Month 6	287.0 (265.0, 310.0)	291.0 (269.0, 319.0)	292.0 (271.0, 322.0)	294.0 (270.0, 326.0)	4.921	0.178
Difference between observed group medians (follow-up - baseline)						
Baseline → Month 1	-7.0	-10.4	-12.0	-13.4	-	-
Baseline → Month 3	-16.0	-23.4	-26.0	-29.4	-	-
Baseline → Month 6	-24.0	-32.4	-36.0	-39.4	-	-
Adjusted geometric mean ratio vs baseline (95% CI)						
Month 1/baseline	0.98 (0.96-1.00)	0.97 (0.95-0.99)	0.96 (0.94-0.98)	0.96 (0.94-0.98)	-	-
Month 3/baseline	0.95 (0.93-0.97)	0.93 (0.91-0.95)	0.92 (0.90-0.94)	0.91 (0.89-0.93)	-	-
Month 6/baseline	0.92 (0.90-0.94)	0.90 (0.88-0.92)	0.89 (0.87-0.91)	0.88 (0.86-0.90)	-	-

Notes: Observed SFCT values are presented as median (25th percentile, 75th percentile). Descriptive changes were calculated as the follow-up median minus the baseline median and were not used for longitudinal inference. Between-phenotype comparisons at individual visits were performed using the Kruskal-Wallis H test. Longitudinal SFCT trajectories were evaluated using linear mixed-effects models fitted to natural log-transformed SFCT values with a patient-specific random intercept. The unadjusted OCT phenotype × time interaction was significant (Wald $\chi^2 = 19.40$, P = 0.022). In the principal adjusted model, age, sex, diabetes duration, HbA1c, systemic glucose-lowering therapy, eGFR, diabetic retinopathy severity, macular ischemia, baseline EZ integrity, and baseline HRF count were included as covariates; the adjusted phenotype × time interaction remained significant (Wald $\chi^2 = 17.30$, P = 0.044). Within-phenotype model-based comparisons with baseline were adjusted using the Bonferroni method. At month 1, the reduction in pure DRT did not remain statistically significant after adjustment (adjusted P = 0.083); reductions in the other three phenotypes were significant (all adjusted P < 0.05). At months 3 and 6, SFCT was significantly lower than baseline in all four phenotypes (all adjusted P < 0.001). CI, confidence interval; CME, cystoid macular edema; DME, diabetic macular edema; DRT, diffuse retinal thickening; eGFR, estimated glomerular filtration rate; EZ, ellipsoid zone; HbA1c, glycated hemoglobin; HRF, hyperreflective foci; OCT, optical coherence tomography; SFCT, subfoveal choroidal thickness; SRD, serous retinal detachment.

Table 6. Ellipsoid zone integrity and within-eye recovery during follow-up according to baseline OCT phenotype

EZ outcome	Overall	Pure DRT	Pure CME	Pure SRD	Mixed DME	χ^2	*p* value
Intact EZ, n/N (%)							
Baseline	103/234 (44.0)	40/60 (66.7)	27/55 (49.1)	17/48 (35.4)	19/71 (26.8)	23.086	< 0.001
Month 1	125/234 (53.4)	45/60 (75.0)	33/55 (60.0)	22/48 (45.8)	25/71 (35.2)	22.756	< 0.001
Month 3	153/234 (65.4)	50/60 (83.3)	39/55 (70.9)	28/48 (58.3)	36/71 (50.7)	17.097	< 0.001
Month 6	174/234 (74.4)	54/60 (90.0)	43/55 (78.2)	34/48 (70.8)	43/71 (60.6)	15.520	0.001
EZ recovery among eyes disrupted at baseline, n/N (%)[†]							
Month 1	26/131 (19.8)	6/20 (30.0)	7/28 (25.0)	6/31 (19.4)	7/52 (13.5)	3.101	0.376
Month 3	54/131 (41.2)	11/20 (55.0)	13/28 (46.4)	12/31 (38.7)	18/52 (34.6)	2.898	0.408
Month 6	72/131 (55.0)	14/20 (70.0)	16/28 (57.1)	17/31 (54.8)	25/52 (48.1)	2.877	0.411

Notes: EZ integrity was assessed at the individual-eye level at baseline and each follow-up visit. [†]EZ recovery was evaluated only among the 131 eyes with EZ disruption at baseline and required a documented disrupted-to-intact transition in the same eye. Cross-sectional comparisons among OCT phenotypes were performed using the Pearson χ^2 test or Fisher's exact test, as appropriate. Longitudinal EZ integrity was evaluated using a binomial GEE model; the time effect was significant (Wald $\chi^2 = 19.60$, $P < 0.001$), whereas the phenotype × time interaction was not significant (Wald $\chi^2 = 1.12$, $P = 0.999$). In the baseline-disrupted subgroup, recovery increased significantly over time (Wald $\chi^2 = 11.36$, $P = 0.003$), without a significant phenotype × time interaction (Wald $\chi^2 = 0.86$, $P = 0.990$). CME, cystoid macular edema; DME, diabetic macular edema; DRT, diffuse retinal thickening; EZ, ellipsoid zone; GEE, generalized estimating equation; OCT, optical coherence tomography; SRD, serous retinal detachment.

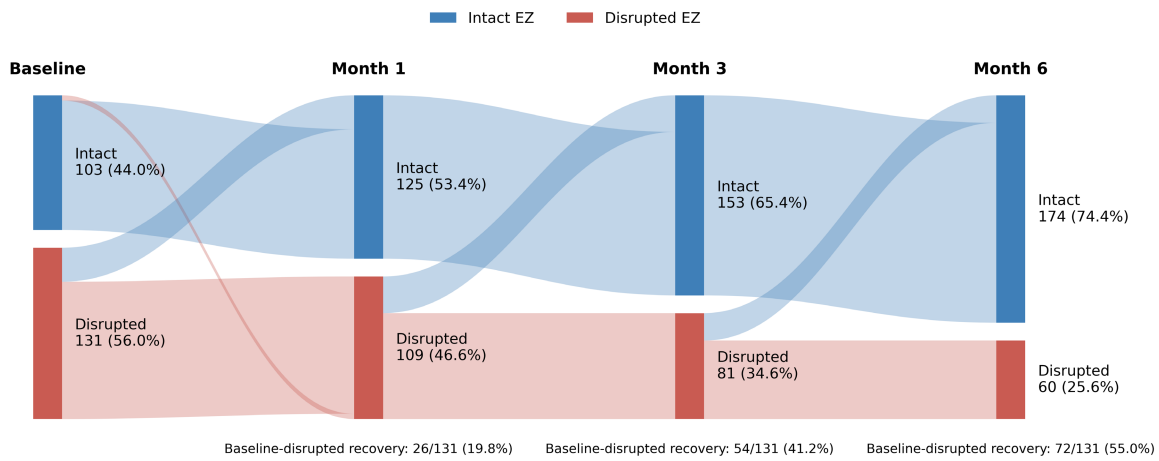


Figure 4. Individual-eye longitudinal transitions in ellipsoid zone integrity during intravitreal conbercept treatment. The alluvial plot illustrates transitions between intact and disrupted EZ status from baseline through months 1, 3, and 6, including persistence of baseline status and restoration of EZ integrity among eyes with baseline disruption. EZ, ellipsoid zone.

line at months 3 and 6 in all groups; at month 1, the reduction was significant in pure CME, pure SRD, and mixed DME but not pure DRT after multiplicity adjustment.

The baseline between-phenotype difference ($H = 8.229$, $P = 0.042$) diminished during follow-up and was no longer significant at months 1, 3, or 6 (all $P > 0.05$). After multivariable adjustment, the phenotype × time interaction remained significant (Wald $\chi^2 = 17.30$, $P = 0.044$), with slightly greater proportional reductions in pure SRD and mixed DME (**Figure 3C**).

Ellipsoid zone integrity and within-eye recovery

EZ integrity improved during follow-up, with persistent differences among OCT phenotypes (**Table 6**). The proportion of eyes with an intact EZ increased from 44.0% at baseline to 74.4% at month 6. At baseline, intact EZ was most frequent in pure DRT (66.7%) and least frequent in mixed DME (26.8%) ($\chi^2 = 23.086$, $P < 0.001$); corresponding month-6 proportions were 90.0% and 60.6% (overall $\chi^2 = 15.520$, $P = 0.001$). In the GEE analysis, EZ integrity increased over time (Wald $\chi^2 = 19.60$, $P < 0.001$), with a significant phenotype effect ($P < 0.001$) but no phenotype × time interaction ($P = 0.999$).

Among 131 eyes with baseline EZ disruption, recovery was observed in 26 (19.8%) at month 1, 54 (41.2%) at month 3, and 72 (55.0%) at month 6. Month-6 recovery ranged from 70.0% in pure DRT to 48.1% in mixed DME. Recovery increased significantly over time (Wald $\chi^2 = 11.36$, $P = 0.003$), whereas the phenotype effect and phenotype × time interaction were not significant (both $P > 0.05$). Individual-eye transitions are shown in Supplementary Table 2 and **Figure 4**.

Among baseline-disrupted eyes, median month-6 BCVA improvement was 0.24 (0.16, 0.34) logMAR with EZ recovery and 0.18 (0.10, 0.29) without recovery ($P = 0.071$). Clinically meaningful visual improvement occurred in 47.2% and 37.3%, respectively ($\chi^2 = 1.31$, $P = 0.253$).

Changes in hyperreflective foci and hard-exudate burden

Total HRF counts decreased from baseline to month 6 in all OCT phenotypes (**Table 7**). Between-phenotype differences were significant at both baseline ($H = 58.161$, $P < 0.001$) and month 6 ($H = 31.442$, $P < 0.001$), with higher counts in pure SRD and mixed DME. The negative binomial GEE showed significant effects of time (Wald $\chi^2 = 118.37$, $P < 0.001$) and phenotype × time (Wald $\chi^2 = 13.72$, $P = 0.003$); inner- and outer-retinal HRF showed similar patterns.

Hard-exudate area decreased from 0.54 to 0.43 mm^2 among 216 eyes with paired gradable photographs. The time effect was significant (Wald $\chi^2 = 5.78$, $P = 0.016$), whereas the

Table 7. Changes in hyperreflective foci and hard-exudate burden and their associations with anatomical and visual changes

Imaging marker	Overall	Pure DRT	Pure CME	Pure SRD	Mixed DME	Test statistic	*p* value
Total HRF count							
Baseline	23.0 (16.0, 30.0)	16.0 (11.0, 21.0)	20.0 (15.0, 26.5)	26.5 (21.5, 33.2)	28.0 (21.0, 38.0)	H = 58.161	< 0.001
Month 6	14.0 (9.0, 20.0)	11.0 (7.0, 15.0)	13.0 (9.0, 18.0)	16.0 (11.0, 22.0)	17.0 (12.0, 24.0)	H = 31.442	< 0.001
Change, M6 - baseline	-8.0 (-13.0, -4.0)	-5.0 (-9.0, -2.0)	-7.0 (-11.0, -3.0)	-10.0 (-15.0, -5.0)	-11.0 (-17.0, -6.0)	H = 18.740	< 0.001
Inner-retinal HRF count							
Baseline	12.0 (8.0, 16.0)	9.0 (6.0, 12.0)	11.0 (8.0, 14.0)	14.0 (10.0, 18.0)	15.0 (10.0, 20.0)	H = 46.218	< 0.001
Month 6	8.0 (5.0, 11.0)	7.0 (4.0, 9.0)	8.0 (5.0, 10.0)	9.0 (6.0, 12.0)	10.0 (6.0, 13.0)	H = 14.763	0.002
Change, M6 - baseline	-4.0 (-7.0, -2.0)	-2.0 (-5.0, -1.0)	-3.0 (-6.0, -1.0)	-4.0 (-8.0, -2.0)	-5.0 (-9.0, -2.0)	H = 12.310	0.006
Outer-retinal HRF count							
Baseline	10.0 (7.0, 14.0)	7.0 (4.0, 10.0)	9.0 (6.0, 12.0)	12.0 (9.0, 16.0)	13.0 (9.0, 18.0)	H = 51.806	< 0.001
Month 6	6.0 (4.0, 9.0)	4.0 (3.0, 6.0)	5.0 (3.0, 8.0)	7.0 (5.0, 10.0)	7.0 (5.0, 11.0)	H = 24.982	< 0.001
Change, M6 - baseline	-4.0 (-7.0, -2.0)	-3.0 (-5.0, -1.0)	-4.0 (-6.0, -2.0)	-6.0 (-9.0, -3.0)	-6.0 (-10.0, -3.0)	H = 15.820	0.001
Hard-exudate area, $mm^{2\dagger}$							
Baseline	0.54 (0.27, 1.11)	0.57 (0.24, 1.07)	0.34 (0.26, 0.78)	0.47 (0.21, 1.31)	0.73 (0.39, 1.17)	H = 6.301	0.098
Month 6	0.43 (0.20, 0.92)	0.44 (0.19, 0.90)	0.28 (0.17, 0.68)	0.39 (0.17, 1.05)	0.61 (0.31, 1.02)	H = 5.987	0.112
Change, M6 - baseline	-0.07 (-0.24, 0.00)	-0.08 (-0.25, 0.00)	-0.05 (-0.19, 0.00)	-0.06 (-0.28, 0.02)	-0.10 (-0.31, 0.01)	H = 2.250	0.522
Change-to-change correlations	r_s (95% CI)						*p* value
ΔHRF vs ΔCMT	0.41 (0.30 to 0.51)	-	-	-	-	-	< 0.001
ΔHRF vs BCVA improvement	-0.26 (-0.38 to -0.14)	-	-	-	-	-	< 0.001
ΔHard-exudate area vs ΔCMT†	0.18 (0.05 to 0.31)	-	-	-	-	-	0.009
ΔHard-exudate area vs BCVA improvement†	-0.12 (-0.25 to 0.01)	-	-	-	-	-	0.076

Notes: Data are presented as median (25th percentile, 75th percentile). Changes in HRF count, hard-exudate area, and CMT were calculated as month-6 minus baseline values; therefore, more negative values indicate greater reductions. BCVA improvement was calculated as baseline minus month-6 logMAR BCVA, such that positive values indicate visual improvement. †Hard-exudate analyses were restricted to 216 eyes with paired gradable baseline and month-6 color fundus photographs (pure DRT, n = 56; pure CME, n = 51; pure SRD, n = 44; mixed DME, n = 65). Between-phenotype comparisons were performed using the Kruskal-Wallis H test. Longitudinal total HRF counts were analyzed using a negative binomial GEE model; the time effect was significant (Wald $\chi^2 = 118.37$, $P < 0.001$), as was the OCT phenotype × time interaction (Wald $\chi^2 = 13.72$, $P = 0.003$). Hard-exudate burden was analyzed using the prespecified transformed linear mixed-effects model; the time effect was significant (Wald $\chi^2 = 5.78$, $P = 0.016$), whereas the phenotype × time interaction was not (Wald $\chi^2 = 1.41$, $P = 0.703$). Correlations were evaluated using Spearman rank correlation coefficients. BCVA, best-corrected visual acuity; CI, confidence interval; CME, cystoid macular edema; CMT, central macular thickness; DME, diabetic macular edema; DRT, diffuse retinal thickening; GEE, generalized estimating equation; HRF, hyperreflective foci; OCT, optical coherence tomography; SRD, serous retinal detachment.

Table 8. Longitudinal changes in systemic inflammatory indices and their associations with ocular changes

Measure	Overall	Pure DRT	Pure CME	Pure SRD	Mixed DME	H statistic	*p* value
SII							
Baseline	596.93 (467.48, 814.17)	594.36 (482.80, 726.48)	656.18 (495.95, 833.36)	586.54 (463.09, 744.60)	603.28 (424.96, 839.54)	2.733	0.435
Month 1	526.84 (403.70, 698.61)	515.47 (406.22, 671.36)	550.63 (420.84, 718.29)	522.76 (399.54, 689.85)	528.32 (393.74, 711.69)	1.367	0.713
Month 3	451.62 (338.26, 606.17)	438.28 (343.36, 579.41)	467.95 (350.27, 620.72)	455.63 (341.18, 592.50)	447.41 (320.64, 628.53)	1.042	0.791
Month 6	410.75 (303.61, 554.88)	396.24 (308.75, 527.46)	421.67 (314.82, 571.09)	419.84 (309.91, 552.14)	411.20 (286.54, 568.78)	1.318	0.725
PIV							
Baseline	236.38 (169.51, 319.69)	222.91 (177.75, 304.31)	225.88 (158.96, 318.24)	259.35 (176.46, 318.80)	239.03 (173.30, 324.18)	1.562	0.668
Month 1	194.73 (137.91, 267.84)	184.65 (134.73, 252.18)	189.77 (138.15, 265.23)	209.46 (145.70, 285.84)	196.23 (139.54, 272.65)	1.715	0.634
Month 3	164.86 (112.93, 225.70)	154.28 (109.84, 211.63)	160.34 (112.27, 221.42)	180.17 (119.63, 239.84)	165.82 (113.40, 229.67)	2.031	0.566
Month 6	148.21 (98.76, 204.58)	137.69 (95.18, 190.42)	145.84 (99.61, 202.75)	163.27 (104.73, 220.36)	150.28 (97.86, 208.41)	2.612	0.455

Notes: Data are presented as median (25th percentile, 75th percentile). Complete blood count data sufficient for calculation of SII and PIV were available for 234 patients at baseline, 227 at month 1, 224 at month 3, and 219 at month 6. The corresponding numbers of available observations in the pure DRT, pure CME, pure SRD, and mixed DME groups were 60/55/48/71 at baseline, 58/53/46/70 at month 1, 57/53/46/68 at month 3, and 56/52/45/66 at month 6, respectively. Between-phenotype comparisons at individual assessment times were performed using the Kruskal-Wallis H test. Longitudinal trajectories were analyzed using linear mixed-effects models fitted to natural log-transformed values. For SII, the time effect was significant (Wald $\chi^2 = 84.67$, $P < 0.001$), whereas the phenotype × time interaction was not significant (Wald $\chi^2 = 6.03$, $P = 0.737$). For PIV, the time effect was significant (Wald $\chi^2 = 111.24$, $P < 0.001$), whereas the phenotype × time interaction was not significant (Wald $\chi^2 = 4.77$, $P = 0.854$). CME, cystoid macular edema; DME, diabetic macular edema; DRT, diffuse retinal thickening; OCT, optical coherence tomography; PIV, pan-immune-inflammation value; SII, systemic immune-inflammation index; SRD, serous retinal detachment.

Table 9. Sequential multivariable models for longitudinal CMT and BCVA trajectories

Outcome	Model	Phenotype × time Wald χ^2	*p* value	Pure DRT	Pure CME	Pure SRD	Mixed DME
CMT	Model 1	156.42	< 0.001	0.75	0.66	0.60	0.57
	Model 2	144.31	< 0.001	0.75	0.66	0.61	0.58
	Model 3	136.84	< 0.001	0.76	0.67	0.62	0.59
	Model 4	120.72	< 0.001	0.77	0.69	0.64	0.61
	Model 5	114.85	< 0.001	0.77	0.70	0.65	0.62
BCVA	Model 1	29.84	< 0.001	-0.29	-0.26	-0.21	-0.19
	Model 2	24.82	0.003	-0.29	-0.25	-0.21	-0.18
	Model 3	21.50	0.011	-0.28	-0.25	-0.20	-0.18
	Model 4	17.70	0.039	-0.26	-0.24	-0.20	-0.18
	Model 5	17.10	0.047	-0.26	-0.23	-0.19	-0.17

Notes: Values in the four phenotype columns represent the model-estimated month-6 effect relative to baseline. For CMT, values are back-transformed geometric mean ratios; values < 1 indicate lower CMT than at baseline. For BCVA, values are adjusted mean changes in logMAR BCVA from baseline to month 6; negative values indicate visual improvement. Model 1 included OCT phenotype, time, and phenotype × time. Model 2 additionally adjusted for age, sex, diabetes duration, HbA1c, and systemic glucose-lowering therapy. Model 3 further adjusted for eGFR, diabetic retinopathy severity, and macular ischemia. Model 4 additionally included baseline EZ integrity, ELM disruption length, cumulative DRIL extent, and total HRF count and was used as the principal structural-adjusted model. Model 5 additionally included cumulative conbercept injection number before each follow-up visit as a time-varying treatment-exposure covariate. Multivariable estimates were pooled across 30 multiply imputed datasets. BCVA, best-corrected visual acuity; CME, cystoid macular edema; CMT, central macular thickness; DME, diabetic macular edema; DRIL, disorganization of the retinal inner layers; DRT, diffuse retinal thickening; eGFR, estimated glomerular filtration rate; ELM, external limiting membrane; EZ, ellipsoid zone; HbA1c, glycated hemoglobin; HRF, hyperreflective foci; OCT, optical coherence tomography; SRD, serous retinal detachment.

phenotype × time interaction and between-phenotype differences at baseline, month 6, and for change were not significant (all P > 0.05).

Changes in manually counted HRF correlated with changes in CMT (r_s = 0.41, P < 0.001) and BCVA improvement (r_s = -0.26, P < 0.001). Hard-exudate reduction was weakly associated with CMT reduction (r_s = 0.18, P = 0.009) but not with BCVA improvement (r_s = -0.12, P = 0.076).

Changes in systemic inflammatory indices and systemic-ocular associations

Both SII and PIV decreased during follow-up (**Table 8**); paired CBC data were available for 234 patients at baseline and 219 at month 6. For SII, the time effect was significant (Wald χ^2 = 84.67, P < 0.001), whereas the phenotype effect and phenotype × time interaction were not (P = 0.406 and P = 0.737, respectively). PIV showed a similar pattern, with a significant time effect (Wald χ^2 = 111.24, P < 0.001) but no phenotype effect or interaction (P = 0.611 and P = 0.854).

From baseline to month 6, changes in SII correlated with changes in CMT (r_s = 0.24, P < 0.001) and HRF (r_s = 0.21, P = 0.002), but not hard-exudate area (P = 0.119). Corresponding associations for PIV were weaker for CMT (r_s = 0.17, P = 0.012) and HRF (r_s = 0.15, P = 0.028), with no association with hard-exudate change (P = 0.256).

After multivariable adjustment, higher time-varying SII remained weakly associated with greater CMT (β = 0.024, 95% CI 0.003-0.045; P = 0.026), whereas PIV was not (β = 0.014, 95% CI -0.005 to 0.033; P = 0.148). Neither index was independently associated with repeated BCVA measurements (Supplementary Table 3).

Multivariable adjusted and classification sensitivity analyses

Sequential adjustment reduced the phenotype × time interactions for CMT and BCVA (**Table 9**). For CMT, the interaction remained significant across all five models (all P < 0.001). In the principal structural-adjusted Model 4, which additionally incorporated baseline EZ integrity, ELM disruption length, cumulative DRIL

Table 10. Discriminative performance of baseline structural and systemic markers for 6-month visual improvement

Predictor/model	AUC	95% CI	*p* value
Baseline CMT	0.61	0.54-0.68	0.004
Baseline EZ integrity	0.65	0.58-0.72	< 0.001
Baseline ELM disruption length	0.68	0.61-0.75	< 0.001
Baseline cumulative DRIL extent	0.67	0.60-0.74	< 0.001
Baseline SII	0.56	0.49-0.64	0.103
CMT + EZ integrity + SII	0.69	0.62-0.76	< 0.001
CMT + EZ integrity + ELM disruption length + cumulative DRIL extent	0.74	0.68-0.81	< 0.001
CMT + EZ integrity + ELM disruption length + cumulative DRIL extent + SII	0.75	0.69-0.81	< 0.001

Notes: Clinically meaningful visual improvement was defined as an improvement of ≥ 0.20 logMAR from baseline to month 6 and occurred in 131 of 234 eyes (56.0%). Individual-marker estimates were obtained from separate univariable logistic regression models. Baseline CMT, ELM disruption length, and cumulative DRIL extent were modeled as continuous variables, EZ integrity as a binary variable (intact vs disrupted), and SII as a natural log-transformed continuous variable. For modeling purposes, ELM disruption length was coded as 0 μm in eyes with an intact ELM. The extended structural model included baseline CMT, EZ integrity, ELM disruption length, and cumulative DRIL extent. The integrated model additionally included baseline SII. AUCs were derived from conventional ROC analyses at the fixed 6-month outcome time point. **Figure 5** presents the prespecified ROC and DCA analyses for baseline CMT, EZ integrity, SII, and their original combined model; the additional ELM/DRIL models are reported in **Table 10** only. AUC, area under the receiver operating characteristic curve; CI, confidence interval; CMT, central macular thickness; DRIL, disorganization of the retinal inner layers; ELM, external limiting membrane; EZ, ellipsoid zone; logMAR, logarithm of the minimum angle of resolution; ROC, receiver operating characteristic; SII, systemic immune-inflammation index.

extent, and HRF count, the interaction remained significant (Wald χ^2 = 120.72, P < 0.001). Additional adjustment for cumulative conbercept exposure produced only modest further attenuation (Model 5: Wald χ^2 = 114.85, P < 0.001). Mixed DME and pure SRD retained the greatest proportional month-6 CMT reductions across models.

For BCVA, the phenotype × time interaction decreased from Wald χ^2 = 29.84 (P < 0.001) in Model 1 to 21.50 (P = 0.011) after adjustment for demographic, metabolic, renal, retinopathy-severity, and ischemic factors in Model 3. Further adjustment for baseline retinal microstructural characteristics in Model 4 attenuated the interaction to Wald χ^2 = 17.70 (P = 0.039). The interaction remained significant after additional adjustment for cumulative injection exposure (Model 5: Wald χ^2 = 17.10, P = 0.047). In Model 4, the adjusted month-6 BCVA changes were -0.26, -0.24, -0.20, and -0.18 logMAR in pure DRT, pure CME, pure SRD, and mixed DME, respectively.

Classification sensitivity analyses yielded similar findings. After exclusion of mixed DME, the phenotype × time interaction remained significant in the principal structural-adjusted model for CMT (Wald χ^2 = 84.67, P < 0.001) and BCVA (Wald χ^2 = 13.82, P = 0.032) (Supplementary Table 4). Using the alternative hierarchical three-group classification, the corresponding interactions remained significant for CMT (Wald χ^2 = 111.63, P < 0.001) and BCVA (Wald χ^2 = 14.31, P = 0.026) (Supplementary Table 5). Complete-case analyses in 216 patients were also consistent with the primary analyses (CMT: Wald χ^2 = 109.54, P < 0.001; BCVA: Wald χ^2 = 17.02, P = 0.049).

Exploratory prognostic performance for 6-month visual improvement

Clinically meaningful visual improvement occurred in 131 of 234 eyes (56.0%), including 65.0% of pure DRT, 56.4% of pure CME, 54.2% of pure SRD, and 49.3% of mixed DME eyes.

Baseline CMT, EZ integrity, and SII yielded AUCs of 0.61 (95% CI 0.54-0.68), 0.65 (95% CI 0.58-0.72), and 0.56 (95% CI 0.49-0.64), respectively. Baseline ELM disruption length and cumulative DRIL extent showed somewhat greater discrimination, with AUCs of 0.68 (95% CI 0.61-0.75) and 0.67 (95% CI 0.60-0.74), respectively. The original CMT+EZ+SII model yielded an AUC of 0.69 (95% CI 0.62-0.76) (**Table 10**; **Figure 5A**).

An extended structural model incorporating CMT, EZ integrity, ELM disruption length, and

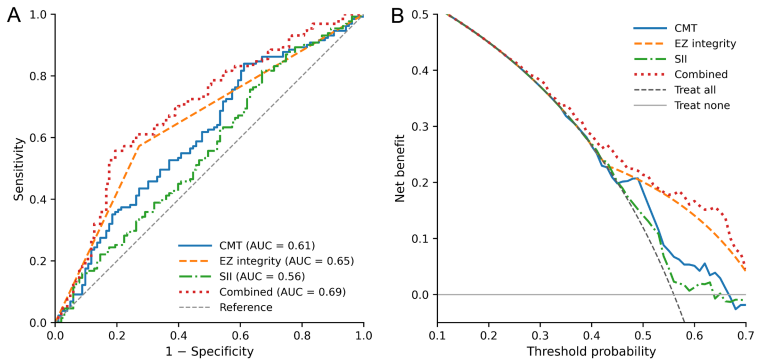


Figure 5. Exploratory prognostic performance of baseline CMT, EZ integrity, and SII for clinically meaningful visual improvement at month 6. A. Receiver operating characteristic curves for baseline CMT, EZ integrity, SII, and the combined CMT+EZ+SII model for discrimination of visual improvement of ≥ 0.20 logMAR at month 6. The corresponding AUCs were 0.61, 0.65, 0.56, and 0.69, respectively. B. Decision-curve analysis comparing the net benefit of the individual-marker and combined models across threshold probabilities. The combined model showed the greatest net benefit across an approximate threshold-probability range of 0.35-0.65, whereas SII alone provided limited incremental net benefit. AUC, area under the receiver operating characteristic curve; CMT, central macular thickness; EZ, ellipsoid zone; logMAR, logarithm of the minimum angle of resolution; ROC, receiver operating characteristic; SII, systemic immune-inflammation index.

cumulative DRIL extent yielded an AUC of 0.74 (95% CI 0.68-0.81). Addition of SII to these structural markers produced only a small further increase in discrimination (AUC, 0.75; 95% CI 0.69-0.81). DCA for the prespecified CMT, EZ, SII, and CMT+EZ+SII models remained unchanged; the combined CMT+EZ+SII model showed greater net benefit than the individual-marker models across threshold probabilities of approximately 0.35-0.65, whereas SII alone provided little additional net benefit (**Figure 5B**).

Anatomy-function mismatch and baseline retinal microstructural characteristics

An anatomical response, defined as a reduction in CMT of > 20% from baseline to month 6, was observed in 200 of 234 eyes (85.5%). The corresponding proportions were 73.3% (44/60) in pure DRT, 87.3% (48/55) in pure CME, 91.7% (44/48) in pure SRD, and 90.1% (64/71) in mixed DME. Anatomy-function mismatch, defined as a CMT reduction of > 20% accompanied by BCVA improvement of < 0.10 logMAR at month 6, occurred in 66 eyes (28.2% of the overall cohort and 33.0% of anatomical responders). The mismatch rates in the overall phenotype groups were 11.7% (7/60) for pure DRT, 23.6% (13/55) for pure CME, 37.5% (18/48) for pure SRD, and 39.4% (28/71) for mixed DME (χ^2 = 15.14, P = 0.002).

Among the 200 anatomical responders, 66 eyes had anatomy-function mismatch and 134 had concordant anatomical and visual responses. Eyes with mismatch more frequently had baseline ELM disruption (75.8% vs 35.8%, P < 0.001) and EZ disruption (72.7% vs 43.3%, P < 0.001) and showed greater ELM disruption length and horizontal, vertical, and cumulative DRIL extent (all P < 0.001) (**Table 11**). Baseline HRF counts were also higher in the mismatch group (P < 0.001). Moderate-to-severe macular ischemia was more frequent among eyes with mismatch (36.4% vs 21.6%, P = 0.025), whereas baseline CMT did not differ significantly between the two response groups (P = 0.073). Baseline BCVA was modestly better in eyes subsequently classified as having mismatch (P = 0.018).

In the multivariable logistic regression restricted to anatomical responders, greater baseline ELM disruption length remained independently associated with anatomy-function mismatch (adjusted OR per 100-μm increase, 1.34; 95% CI 1.12-1.61; P = 0.001), as did greater cumulative DRIL extent (adjusted OR per 100-μm increase, 1.23; 95% CI 1.08-1.40; P = 0.002), after adjustment for baseline BCVA, baseline CMT, macular ischemia, and OCT phenotype. Higher baseline logMAR BCVA was inversely associated with mismatch (adjusted OR per 0.10-logMAR increase, 0.88; 95% CI 0.79-0.98; P = 0.022). Baseline CMT was not independently associated with mismatch (adjusted OR per 100-μm increase, 1.07; 95% CI 0.90-1.28; P = 0.438), and the overall OCT phenotype effect was attenuated after adjustment (P = 0.317).

Discussion

This study characterized changes in anatomical, functional, outer-retinal, local imaging, and

Table 11. Baseline characteristics of anatomical responders according to anatomy-function concordance

Characteristic	Anatomy-function mismatch (n = 66)	Concordant response (n = 134)	Test statistic	*p* value
ELM disrupted, n (%)	50 (75.8)	48 (35.8)	$\chi^2 = 28.50$	< 0.001
ELM disruption length, μm†	382.4 (268.5, 498.7)	0.0 (0.0, 326.1)	Z = -6.21	< 0.001
Horizontal DRIL extent, μm	286.3 (205.4, 370.8)	188.2 (124.7, 272.5)	Z = -5.13	< 0.001
Vertical DRIL extent, μm	248.6 (176.3, 335.4)	166.8 (112.5, 244.1)	Z = -4.72	< 0.001
Cumulative DRIL extent, μm	548.2 (397.1, 703.6)	356.4 (254.0, 503.2)	Z = -5.24	< 0.001
EZ disrupted, n (%)	48 (72.7)	58 (43.3)	$\chi^2 = 15.46$	< 0.001
Total HRF count	28.0 (22.0, 36.0)	21.0 (15.0, 28.0)	Z = -4.37	< 0.001
Baseline BCVA, logMAR	0.70 (0.55, 0.84)	0.80 (0.62, 0.95)	Z = -2.36	0.018
Baseline CMT, μm	512.1 (407.8, 580.6)	481.6 (381.9, 553.2)	Z = -1.79	0.073
Moderate/severe macular ischemia, n (%)	24 (36.4)	29 (21.6)	$\chi^2 = 5.00$	0.025
OCT phenotype, n (%)			$\chi^2 = 11.16$	0.011
Pure DRT	7 (10.6)	37 (27.6)		
Pure CME	13 (19.7)	35 (26.1)		
Pure SRD	18 (27.3)	26 (19.4)		
Mixed DME	28 (42.4)	36 (26.9)		

Notes: Anatomical response was defined as a > 20% reduction in CMT from baseline to month 6. Among anatomical responders, anatomy-function mismatch was defined as a > 20% CMT reduction accompanied by BCVA improvement of < 0.10 logMAR, approximately corresponding to a gain of < 5 ETDRS letters; concordant response was defined as a > 20% CMT reduction accompanied by BCVA improvement of ≥ 0.10 logMAR. Continuous variables are presented as median (25th percentile, 75th percentile) and were compared using the Mann-Whitney U test; categorical variables were compared using the Pearson χ^2 test or Fisher's exact test, as appropriate. †For this analysis, ELM disruption length was coded as 0 μm in eyes with an intact ELM. Cumulative DRIL extent was calculated as the sum of horizontal and vertical DRIL extent. BCVA, best-corrected visual acuity; CME, cystoid macular edema; CMT, central macular thickness; DME, diabetic macular edema; DRIL, disorganization of the retinal inner layers; DRT, diffuse retinal thickening; ELM, external limiting membrane; EZ, ellipsoid zone; HRF, hyperreflective foci; logMAR, logarithm of the minimum angle of resolution; OCT, optical coherence tomography; SRD, serous retinal detachment.

systemic inflammatory parameters during 6 months of intravitreal conbercept treatment across four baseline OCT phenotypes of DME. CMT and BCVA improved in all phenotypes, but their longitudinal trajectories differed. Pure SRD and mixed DME showed the greatest proportional CMT reductions, whereas pure DRT had the most favorable adjusted BCVA trajectory. SFCT also decreased with modest phenotype-specific differences. EZ integrity improved progressively, including restoration in more than half of eyes with baseline disruption. HRF decreased substantially and tracked both CMT reduction and BCVA improvement, whereas hard-exudate changes were smaller. In contrast, SII and PIV declined over time without phenotype-specific trajectories; only SII retained a weak adjusted association with CMT, and neither index was associated with repeated BCVA. These findings remained broadly consistent after sequential covariate adjustment, additional adjustment for injection exposure, and alternative OCT classifications.

Our findings on anatomical and visual improvements are in line with established evidence that supports conbercept for center-involving DME. The phase III Sailing study demonstrated sustained visual and anatomical benefit with conbercept, and a recent study directly comparing OCT morphologic patterns during conbercept treatment also reported meaningful improvement across DRT, CME, and SRD, with differences in visual and anatomical outcomes among patterns [4, 20]. Our study extends these observations by retaining mixed DME as a separate category and by examining longitudinal trajectories rather than isolated post-treatment measurements. Importantly, phenotype × time interactions for both CMT and BCVA persisted after adjustment for metabolic, renal, retinopathy, ischemic, structural, and treatment-exposure variables, suggesting that baseline OCT morphology retains information about subsequent response patterns beyond these measured factors.

The anatomical response did not fully parallel visual recovery. Eyes with pure SRD and mixed DME began with greater CMT and showed larger proportional thickness reductions, yet their visual gains were smaller than those observed in pure DRT. Quantitative OCT studies have similarly shown that the amount and compartment of retinal fluid provide information beyond central thickness alone, while real-world biomarker studies indicate that visual outcomes depend on combinations of fluid morphology, outer-retinal integrity, DRIL, and other structural features [5, 21]. This supports an important clinical distinction: a large reduction in CMT reflects substantial anatomical response but does not necessarily indicate equivalent functional recovery. The persistence of the principal findings after excluding mixed DME and after applying the alternative hierarchical classification also reduces concern that the observed trajectory differences resulted solely from the four-category classification scheme.

SFCT decreased across all four phenotypes, although baseline differences became less evident during follow-up. A recent prospective study of conbercept-treated DME similarly reported progressive SFCT reduction over 6 months alongside improvements in CMT and BCVA, without a clear relationship between SFCT and final visual outcome [22]. Our findings therefore support SFCT as a complementary structural measure rather than a direct surrogate for visual recovery. Because choroidal thickness is influenced by ocular and systemic factors, its interpretation is likely most useful when integrated with retinal fluid morphology, photoreceptor integrity, and visual function.

The longitudinal EZ findings offer insight into outer-retinal recovery. The proportion of eyes with an intact EZ increased from 44.0% at baseline to 74.4% at month 6, and 55.0% of eyes with baseline EZ disruption had restored integrity at month 6. Previous longitudinal studies have shown that reductions in EZ defects accompany anti-VEGF treatment and are associated with visual outcomes [23]. A recent systematic review likewise identified baseline EZ disruption among the OCT features associated with poorer subsequent visual acuity, although the certainty of prognostic evidence remains limited by heterogeneity in biomarker definitions and confounder adjustment [6]. In the present study, BCVA improvement was numerically greater in eyes with EZ recovery, but the difference was not statistically significant. Because EZ integrity was assessed categorically rather than by quantitative defect length, the observed restoration should be interpreted as a temporally concurrent structural change rather than evidence that EZ recovery independently predicts or mediates visual improvement. Binary EZ grading therefore remains an exploratory imaging measure with limited clinical reference value.

HRF exhibited a more dynamic association with treatment response. Counts decreased in all phenotypes, with phenotype-specific differences in the magnitude of change, and greater HRF reduction correlated with both greater CMT reduction and greater BCVA improvement. Previous anti-VEGF studies have linked retinal HRF, particularly outer-retinal HRF, with photoreceptor integrity and visual outcomes in DME [24]. These findings demonstrate parallel changes in manually counted HRF, retinal thickness, and visual function. However, HRF was assessed by manual counting within the central 3-mm region rather than by automated or standardized density measurement within the central 1-mm region. The observed correlations should therefore be regarded as exploratory concurrent relationships rather than evidence of validated quantitative biomarker performance or a specific histological measure of retinal inflammation. Hard exudates showed a different temporal pattern, with only modest reduction and no phenotype-specific trajectory. This is compatible with recent Protocol T analyses showing that hard-exudate burden may change more slowly and nonlinearly after anti-VEGF initiation and has a less consistent relationship with visual improvement [25].

Systemic inflammatory findings showed limited associations with ocular outcomes. SII and PIV decreased over follow-up but did not differ in their longitudinal trajectories among OCT phenotypes. Changes in both indices correlated weakly with CMT and HRF, whereas only time-varying SII retained a small adjusted association with CMT and neither index was independently associated with BCVA. Previous studies have reported associations between SII and OCT-based DME severity or HRF [7], while PIV

has been associated with DME and selected OCT features, including HRF and SRF [26]. These findings indicate limited systemic-ocular covariation rather than evidence of an inflammatory pathway underlying macular edema resolution. SII and PIV are derived from circulating leukocyte and platelet counts and may vary with glycemic status, renal function, concomitant treatment, intercurrent illness, and other systemic factors. Because aqueous or vitreous VEGF, PlGF, IL-6, ICAM-1, and other locally specific mediators were not measured, the observed declines in SII and PIV cannot be attributed specifically to intravitreal conbercept, nor can a mediating relationship between these circulating indices and reduction in macular edema be inferred.

The exploratory prognostic analysis corroborated this pattern. Baseline CMT, EZ integrity, and SII individually showed limited-to-modest discrimination for clinically meaningful month-6 visual improvement, whereas their combination increased the AUC to 0.69 and showed the greatest net benefit across an approximate threshold range of 0.35-0.65. Previous work combining systemic inflammatory indices with OCT biomarkers has likewise shown that multimarker models may outperform isolated systemic indices in predicting anti-VEGF response [27]. Nevertheless, the present analysis was exploratory. An AUC of 0.69 represents only moderate discrimination, and the model was assessed within the same cohort rather than independently validated. The ROC and DCA findings therefore support complementary prognostic information from structural and systemic markers but do not establish a clinical prediction tool.

Although the present clinical study was not designed to elucidate molecular mechanisms, previous experimental evidence provides a biological framework for the observed anatomical changes. Conbercept is a soluble VEGF-receptor decoy that binds multiple VEGF-A isoforms, VEGF-B, and PlGF [28]. Experimental studies under hyperglycemic conditions showed that conbercept suppressed VEGF/PlGF-driven retinal endothelial-cell migration and sprouting through modulation of Src, PI3K/Akt, and ERK signaling [29]. In streptozotocin-induced diabetic rats, conbercept reduced retinal vascular leakage and was accompanied by more preserved vascular occludin and claudin-5 distribution and inhibition of VEGFR2-related Src/PI3K/Akt/ERK signaling [30]. Additional experimental work in diabetic retinopathy has reported reductions in ICAM-1, IL-6, TNF-α, and NF-κB-related signaling after conbercept treatment [31]. By contrast, a clinical DME study found a marked reduction in aqueous VEGF after conbercept but no significant short-term changes in several other measured cytokines, emphasizing that anti-VEGF activity should not be equated with broad anti-inflammatory effects [32]. In this context, the weak association between longitudinal SII and CMT in our cohort may reflect systemic inflammatory status accompanying retinal edema rather than direct systemic target engagement. A testable hypothesis for future investigation is that local VEGF/PlGF blockade improves blood-retinal barrier integrity through VEGFR2-related permeability signaling, whereas systemic inflammatory status may covary with susceptibility to or resolution of retinal edema without necessarily mediating the local treatment effect. Prospective studies combining serial systemic inflammatory indices with paired aqueous or vitreous VEGF, PlGF, IL-6, and ICAM-1 measurements, retinal barrier markers, and OCT phenotyping are required to determine whether systemic and intraocular inflammatory changes are biologically linked.

Several features strengthen the study. The four-category OCT definition preserved mixed morphology rather than automatically incorporating all SRD-containing eyes into one group; imaging assessments showed high intergrader reliability; and repeated-measures analyses incorporated longitudinal observations while adjusting for clinically relevant metabolic, renal, ischemic, retinal, and treatment-exposure variables. The consistency of CMT and BCVA findings across the pure-pattern, alternative-classification, treatment-exposure, and complete-case analyses further supports the robustness of the main trajectory findings. Simultaneous assessment of CMT, BCVA, SFCT, EZ transitions, HRF, hard exudates, SII, and PIV also allowed direct comparison of local structural and systemic changes within the same cohort.

Several limitations of this work remain. First, the retrospective single-center design introduces potential selection bias, residual confound-

ing, and limited generalizability. Eligibility required completion of the loading regimen and sufficient 6-month outcome ascertainment, which may further select for patients with better treatment continuity. Second, the study lacked an untreated or active-comparator control group, because all included eyes received conbercept. Consequently, the observed structural and functional changes cannot be attributed exclusively to conbercept, and the contributions of the natural course of DME, regression to the mean, concurrent systemic management, or other time-varying factors cannot be fully separated from treatment-related effects. The study therefore evaluates heterogeneity within a conbercept-treated cohort rather than comparative or causal treatment efficacy. Third, the 6-month follow-up does not capture longer-term recurrence, cumulative treatment burden, or delayed structural recovery. Fourth, although baseline ELM disruption length and horizontal, vertical, and cumulative DRIL extent were quantitatively assessed, EZ integrity remained a categorical manual measure and HRF was manually counted within the central 3-mm region. Quantitative EZ defect length, standardized foveal neuroretina-to-RPE optical-density ratios, and absolute central 1-mm HRF density were not available. These limitations restrict the quantitative precision and clinical reference value of the EZ and HRF findings, which should be regarded as hypothesis-generating. Fifth, aqueous and vitreous concentrations of VEGF, PlGF, IL-6, ICAM-1, and other locally specific mediators were not measured. Consequently, the temporal changes in circulating SII and PIV cannot be linked directly to intraocular inflammatory activity, and no causal mediation between systemic inflammatory indices and macular edema resolution can be inferred. Finally, the exploratory ROC and DCA analyses require independent validation before any prognostic application.

Future translational studies should adopt a prospective multicenter design with predefined imaging and biospecimen protocols. A practical implementation framework would include enrollment of conbercept-treated patients together with an appropriate contemporaneous comparator cohort, standardized OCT acquisition across centers, and centralized quantitative assessment of parameters such as CMT, ELM disruption length, DRIL extent, EZ defect length, and central HRF density. Peripheral blood and paired aqueous humor, and vitreous samples when clinically available, should be collected at predefined treatment time points for measurement of VEGF, PlGF, IL-6, ICAM-1, and related mediators. Linking these serial molecular measurements with quantitative OCT trajectories and visual outcomes would allow separation of systemic from intraocular inflammatory changes and provide a stronger basis for testing whether specific molecular pathways mediate structural and functional response to anti-VEGF therapy.

Overall, the findings indicate that OCT morphology captures clinically relevant heterogeneity in the anatomical and functional course of conbercept-treated DME, but morphology alone is insufficient to characterize treatment response. Pure SRD and mixed DME showed pronounced anatomical improvement, whereas pure DRT had the most favorable visual trajectory. ELM and DRIL provided quantitative information on retinal microstructural integrity, whereas categorical EZ assessment and manually counted HRF showed exploratory concurrent changes during follow-up. Circulating inflammatory indices showed weaker relationships with ocular outcomes. These results support a multidimensional interpretation of DME response integrating morphology, outer-retinal integrity, local imaging biomarkers, and visual function rather than reliance on CMT or systemic inflammatory markers alone.

Conclusion

Over the 6-month treatment period, anatomical and visual outcomes improved across all OCT phenotypes, albeit with different trajectories. Pure SRD and mixed DME showed greater CMT reductions, whereas pure DRT had the most favorable visual trajectory. Categorically assessed EZ integrity improved progressively, while manually counted HRF declined concurrently with anatomical and visual improvement; these findings remain exploratory and require confirmation using quantitative OCT metrics. SII and PIV showed predominantly nonspecific temporal changes and limited prognostic discrimination. Combined structural and systemic markers provided modestly improved prognostic performance but remain exploratory. Prospective multicenter studies incorporating

appropriate comparator groups, standardized quantitative OCT, and paired systemic and intraocular biomarker sampling are needed to validate these measures for individualized prognostic stratification.

Acknowledgements

This study was supported by the Jilin Provincial Department of Education Science and Technology Research Project (No. JJKH20220072KJ).

Disclosure of conflict of interest

None.

Address correspondence to: Xiangjun Li, Department of Ophthalmology, The Affiliated Hospital of Bei-hua University, No. 12, Jiefang Middle Road, Jilin 132011, Jilin, China. E-mail: xiangjun777@126.com

References

[1] Teo ZL, Tham YC, Yu M, Chee ML, Rim TH, Cheung N, Bikbov MM, Wang YX, Tang Y, Lu Y, Wong IY, Ting DSW, Tan GSW, Jonas JB, Sabanayagam C, Wong TY and Cheng CY. Global prevalence of diabetic retinopathy and projection of burden through 2045: systematic review and meta-analysis. Ophthalmology 2021; 128: 1580-1591.

[2] Im JHB, Jin YP, Chow R and Yan P. Prevalence of diabetic macular edema based on optical coherence tomography in people with diabetes: a systematic review and meta-analysis. Surv Ophthalmol 2022; 67: 1244-1251.

[3] Figueira J, Henriques J, Carneiro Â, Marques-Neves C, Flores R, Castro-Sousa JP, Meireles A, Gomes N, Nascimento J, Amaro M and Silva R. Guidelines for the management of center-involving diabetic macular edema: treatment options and patient monitorization. Clin Ophthalmol 2021; 15: 3221-3230.

[4] Szeto SK, Hui VWK, Tang FY, Yang D, Sun ZH, Mohamed S, Chan CKM, Lai TYY and Cheung C. OCT-based biomarkers for predicting treatment response in eyes with centre-involved diabetic macular oedema treated with anti-VEGF injections: a real-life retina clinic-based study. Br J Ophthalmol 2023; 107: 525-533.

[5] Liu K, Wang H, He W, Ye J, Song Y, Wang Y, Liu X, Wu Z, Chen S, Fan K, Liu Y, Zhang F, Li Z, Liu L, Zhang J, Zhang X, Ye J, Liang X, Li X, Ke X, Wu Q, Li J, Tao S, Wang X, Rosenfeld P, Heier JS, Kaiser P and Xu X. Intravitreal conbercept for diabetic macular oedema: 2-year results from a randomised controlled trial and open-label extension study. Br J Ophthalmol 2022; 106: 1436-1443.

[6] Nanji K, Hatamnejad A, Grad J, El-Sayes A, Mihalache A, Gemae M, Huang R, Phillips M, Zeraatkar D, Singh R, Munk MR, Sadda SR, Sarraf D, Kaiser P, Guymer R, Sivaprasad S, Fraser-Bell S, Tham YC, Garg SJ, Wong TY, Wykoff CC and Chaudhary V. Visual outcomes associated with optical coherence tomography biomarkers in diabetic macular edema: a systematic review. Surv Ophthalmol 2026; 71: 289-308.

[7] Yanxia C, Xiongyi Y, Min F and Xiaoyun K. Optical coherence tomography-based grading of diabetic macular edema is associated with systemic inflammatory indices and imaging biomarkers. Ophthalmic Res 2024; 67: 96-106.

[8] Candan O, Orman G, Ünlü N and Ozkan G. Diagnostic efficiency of pan-immune-inflammation value to predict diabetic macular edema and its relationship with OCT-based biomarkers of inflammation. Int Ophthalmol 2025; 45: 365.

[9] von Elm E, Altman DG, Egger M, Pocock SJ, Gøtzsche PC and Vandenbroucke JP; STROBE Initiative. The Strengthening the Reporting of Observational Studies in Epidemiology (STROBE) statement: guidelines for reporting observational studies. Lancet 2007; 370: 1453-1457.

[10] Ren F, Zhang X, Gong H, Tian X, Kong X, Hu Y, Yang J, Shi W, Zhang H, Zhou L and Zhang G. Two different initial treatment regimens of conbercept in diabetic macular edema: 12-month results from a multicenter randomized controlled study. Photodiagnosis Photodyn Ther 2023; 44: 103745.

[11] Otani T, Kishi S and Maruyama Y. Patterns of diabetic macular edema with optical coherence tomography. Am J Ophthalmol 1999; 127: 688-693.

[12] Kim BY, Smith SD and Kaiser PK. Optical coherence tomographic patterns of diabetic macular edema. Am J Ophthalmol 2006; 142: 405-412.

[13] Avery RL, Bakri SJ, Blumenkranz MS, Brucker AJ, Cunningham ET Jr, D'Amico DJ, Dugel PU, Flynn HW Jr, Freund KB, Haller JA, Jumper JM, Liebmann JM, McCannel CA, Mieler WF, Ta CN and Williams GA. Intravitreal injection technique and monitoring: updated guidelines of an expert panel. Retina 2014; 34: S1-S18.

[14] Wilkinson CP, Ferris FL 3rd, Klein RE, Lee PP, Agardh CD, Davis M, Dills D, Kampik A, Pararajasegaram R and Verdaguer JT; Global Diabetic Retinopathy Project Group. Proposed international clinical diabetic retinopathy and diabetic macular edema disease severity scales. Ophthalmology 2003; 110: 1677-1682.

[15] Sim DA, Keane PA, Zarranz-Ventura J, Fung S, Powner MB, Platteau E, Bunce CV, Fruttiger M, Patel PJ, Tufail A and Egan CA. The effects of

macular ischemia on visual acuity in diabetic retinopathy. Invest Ophthalmol Vis Sci 2013; 54: 2353-2360.
[16] De S, Saxena S, Kaur A, Mahdi AA, Misra A, Singh M, Meyer CH and Akduman L. Sequential restoration of external limiting membrane and ellipsoid zone after intravitreal anti-VEGF therapy in diabetic macular oedema. Eye (Lond) 2021; 35: 1490-1495.
[17] Huang CH, Yang CH, Hsieh YT, Yang CM, Ho TC and Lai TT. Hyperreflective foci in predicting the treatment outcomes of diabetic macular oedema after anti-vascular endothelial growth factor therapy. Sci Rep 2021; 11: 5103.
[18] Domalpally A, Ip MS and Ehrlich JS. Effects of intravitreal ranibizumab on retinal hard exudate in diabetic macular edema: findings from the RIDE and RISE phase III clinical trials. Ophthalmology 2015; 122: 779-786.
[19] Hsieh TC, Deng GH, Chang YC, Chang FL and He MS. A real-world study for timely assessing the diabetic macular edema refractory to intravitreal anti-VEGF treatment. Front Endocrinol (Lausanne) 2023; 14: 1108097.
[20] Shi XN, Zhang QY, Ju CJ, Xu YC and Xiong ZH. Efficacy of anti-VEGF therapy for different OCT patterns in diabetic macular edema and the correlation between ellipsoid zone integrity and visual acuity. Sci Rep 2026; 16: 15903.
[21] Roberts PK, Vogl WD, Gerendas BS, Glassman AR, Bogunovic H, Jampol LM and Schmidt-Erfurth UM. Quantification of fluid resolution and visual acuity gain in patients with diabetic macular edema using deep learning: a post hoc analysis of a randomized clinical trial. JAMA Ophthalmol 2020; 138: 945-953.
[22] Shi XN, Zhang QY, Ju CJ, Xu YC and Xiong ZH. Effects of anti-VEGF therapy on choroidal thickness in eyes with diabetic macular edema. BMC Ophthalmol 2026; 26: 261.
[23] Sharef N, Kassem R, Hecht I, Bar A, Maharshak I, Burgansky-Eliash Z, Weinberger Y, Tuuminen R and Achiron A. Interdigitation and ellipsoid zones disruption correlate with visual outcomes among treatment-naive patients with diabetic macular edema. Ophthalmic Res 2021; 64: 476-482.
[24] Tang L, Luo D, Qiu Q, Xu GT and Zhang J. Hyperreflective foci in diabetic macular edema with subretinal fluid: association with visual outcomes after anti-VEGF treatment. Ophthalmic Res 2023; 66: 39-47.
[25] Pak K, Yoon C and Sadda SR. Hard exudates in diabetic macular edema after intravitreal anti-VEGF therapy: a post-hoc analysis of the DRCR protocol T trial. Graefes Arch Clin Exp Ophthalmol 2026; 264: 427-436.
[26] Candan O, Orman G, Ünlü N and Ozkan G. Diagnostic efficiency of pan-immune-inflammation value to predict diabetic macular edema and its relationship with OCT-based biomarkers of inflammation. Int Ophthalmol 2025; 45: 365.
[27] Ergin E, Dascalu AM, Stana D, Tribus LC, Arsene AL, Nedea MI, Serban D, Nistor CE, Tudor C, Dumitrescu D, Stoica PL and Cristea BM. Predictive role of complete blood count-derived inflammation indices and optical coherence tomography biomarkers for early response to intravitreal anti-VEGF in diabetic macular edema. Biomedicines 2025; 13: 1308.
[28] Wang Q, Li T, Wu Z, Wu Q, Ke X, Luo D and Wang H. Novel VEGF decoy receptor fusion protein conbercept targeting multiple VEGF isoforms provide remarkable anti-angiogenesis effect in vivo. PLoS One 2013; 8: e70544.
[29] Chen X, Li J, Li M, Zeng M, Li T, Xiao W, Li J, Wu Q, Ke X, Luo D, Tang S and Luo Y. KH902 suppresses high glucose-induced migration and sprouting of human retinal endothelial cells by blocking VEGF and PlGF. Diabetes Obes Metab 2013; 15: 224-233.
[30] Huang J, Li X, Li M, Li S, Xiao W, Chen X, Cai M, Wu Q, Luo D, Tang S and Luo Y. Effects of intravitreal injection of KH902, a vascular endothelial growth factor receptor decoy, on the retinas of streptozotocin-induced diabetic rats. Diabetes Obes Metab 2012; 14: 644-653.
[31] Xia JP, Liu SQ and Wang S. Intravitreal conbercept improves outcome of proliferative diabetic retinopathy through inhibiting inflammation and oxidative stress. Life Sci 2021; 265: 118795.
[32] Wei Q, Wan Z, Hu Y and Peng Q. Cytokine and chemokine profile changes in patients after intravitreal conbercept injection for diabetic macular edema. Drug Des Devel Ther 2019; 13: 4367-4374.

Supplementary Table 1. Composition of the mixed DME phenotype at baseline

Mixed OCT component combination	n	% of mixed DME (n = 71)	% of overall cohort (N = 234)
DRT + CME	31	43.7	13.2
DRT + SRD	17	23.9	7.3
CME + SRD	14	19.7	6.0
DRT + CME + SRD	9	12.7	3.8
Total mixed DME	71	100.0	30.3

Notes: Mixed DME was defined by the presence of two or more of the three prespecified OCT morphologic components. Percentages in the third column use the 71 mixed DME eyes as the denominator; percentages in the fourth column use the entire 234-eye cohort as the denominator. CME, cystoid macular edema; DME, diabetic macular edema; DRT, diffuse retinal thickening; OCT, optical coherence tomography; SRD, serous retinal detachment.

Supplementary Table 2. Individual-eye transitions in ellipsoid zone integrity from baseline to follow-up

Follow-up	OCT phenotype	Intact→Intact, n (%)	Intact→Disrupted, n (%)	Disrupted→Intact, n (%)	Disrupted→Disrupted, n (%)
Month 1	Pure DRT	39 (65.0)	1 (1.7)	6 (10.0)	14 (23.3)
	Pure CME	26 (47.3)	1 (1.8)	7 (12.7)	21 (38.2)
	Pure SRD	16 (33.3)	1 (2.1)	6 (12.5)	25 (52.1)
	Mixed DME	18 (25.4)	1 (1.4)	7 (9.9)	45 (63.4)
Month 3	Pure DRT	39 (65.0)	1 (1.7)	11 (18.3)	9 (15.0)
	Pure CME	26 (47.3)	1 (1.8)	13 (23.6)	15 (27.3)
	Pure SRD	16 (33.3)	1 (2.1)	12 (25.0)	19 (39.6)
	Mixed DME	18 (25.4)	1 (1.4)	18 (25.4)	34 (47.9)
Month 6	Pure DRT	40 (66.7)	0 (0.0)	14 (23.3)	6 (10.0)
	Pure CME	27 (49.1)	0 (0.0)	16 (29.1)	12 (21.8)
	Pure SRD	17 (35.4)	0 (0.0)	17 (35.4)	14 (29.2)
	Mixed DME	18 (25.4)	1 (1.4)	25 (35.2)	27 (38.0)

Notes: Each row represents the transition of the same eye from its baseline EZ status to the indicated follow-up visit. Percentages use the total number of eyes within each OCT phenotype as the denominator. Thus, Intact→Intact plus Intact→Disrupted equals the number of eyes with an intact EZ at baseline, whereas Disrupted→Intact plus Disrupted→Disrupted equals the number of eyes with baseline EZ disruption. CME, cystoid macular edema; DME, diabetic macular edema; DRT, diffuse retinal thickening; EZ, ellipsoid zone; OCT, optical coherence tomography; SRD, serous retinal detachment.

Supplementary Table 3. Adjusted longitudinal associations of systemic inflammatory indices with CMT and BCVA

Dependent outcome	Time-varying explanatory variable	Adjusted β	95% CI	*p* value
ln(CMT)	ln(SII)	0.024	0.003 to 0.045	0.026
ln(CMT)	ln(PIV)	0.014	-0.005 to 0.033	0.148
BCVA, logMAR	ln(SII)	0.011	-0.005 to 0.027	0.176
BCVA, logMAR	ln(PIV)	0.006	-0.008 to 0.020	0.401

Notes: Separate linear mixed-effects models were fitted for each systemic inflammatory index and ocular outcome. Models included a patient-specific random intercept and were adjusted for baseline OCT phenotype, assessment time, age, sex, diabetes duration, HbA1c, eGFR, macular ischemia, and systemic glucose-lowering therapy. SII and PIV were entered as time-varying natural log-transformed variables. CMT was analyzed on the natural log scale, whereas BCVA was analyzed on the logMAR scale. β therefore represents the adjusted change in the dependent outcome associated with a one-unit increase in the natural logarithm of the corresponding systemic inflammatory index. BCVA, best-corrected visual acuity; CI, confidence interval; CMT, central macular thickness; eGFR, estimated glomerular filtration rate; HbA1c, glycated hemoglobin; PIV, pan-immune-inflammation value; SII, systemic immune-inflammation index.

Supplementary Table 4. Pure-phenotype sensitivity analysis excluding mixed DME

Outcome	Pure DRT	Pure CME	Pure SRD	Phenotype × time Wald χ^2	*p* value
CMT, month-6 geometric mean ratio vs baseline	0.76	0.67	0.62	92.14	< 0.001
BCVA, adjusted mean change at month 6, logMAR	-0.28	-0.25	-0.20	15.41	0.017

Notes: The sensitivity analysis included 163 eyes after exclusion of the 71 mixed DME eyes: pure DRT, n = 60; pure CME, n = 55; and pure SRD, n = 48. Estimates were obtained from the principal adjusted Model 3, including age, sex, diabetes duration, HbA1c, systemic glucose-lowering therapy, eGFR, diabetic retinopathy severity, macular ischemia, baseline EZ integrity, and baseline HRF count. CMT values are geometric mean ratios comparing month 6 with baseline; BCVA values are adjusted mean changes from baseline to month 6, with negative values indicating improvement. BCVA, best-corrected visual acuity; CME, cystoid macular edema; CMT, central macular thickness; DRT, diffuse retinal thickening; eGFR, estimated glomerular filtration rate; EZ, ellipsoid zone; HbA1c, glycated hemoglobin; HRF, hyperreflective foci; SRD, serous retinal detachment.

Supplementary Table 5. Sensitivity analysis using the alternative hierarchical OCT classification

Outcome	DRT group (n = 60)	CME group (n = 86)	SRD group (n = 88)	Group × time Wald χ^2	*p* value
CMT, month-6 geometric mean ratio vs baseline	0.76	0.66	0.60	121.54	< 0.001
BCVA, adjusted mean change at month 6, logMAR	-0.28	-0.24	-0.19	17.02	0.009

Notes: Under the alternative hierarchical classification, eyes with DRT alone remained in the DRT group; eyes with CME, including DRT+CME without SRD, were classified as CME; and all eyes containing SRD were classified as SRD. Accordingly, the 31 DRT+CME mixed eyes were reassigned to CME, whereas the 17 DRT+SRD, 14 CME+SRD, and 9 DRT+CME+SRD eyes were reassigned to SRD. Estimates were obtained from the principal adjusted Model 3. CMT values are geometric mean ratios comparing month 6 with baseline; BCVA values are adjusted mean changes from baseline to month 6, with negative values indicating improvement. BCVA, best-corrected visual acuity; CME, cystoid macular edema; CMT, central macular thickness; DRT, diffuse retinal thickening; OCT, optical coherence tomography; SRD, serous retinal detachment.